

AD83232

ZR-658-030
AERODYNAMICS

A REVIEW OF SHOCK TUBES AND SHOCK TUNNELS

BY
W. A. MARTIN

CONVAIR-
ASTRONAUTICS
JUN 10 1959
LIBRARY

A13773

e. 8

AD832325

Report No. ZR-658-050

CONVAIR-
ASTRONAUTICS
JUN 10 1959
LIBRARY

A REVIEW OF SHOCK TUBES
AND SHOCK TUNNELS

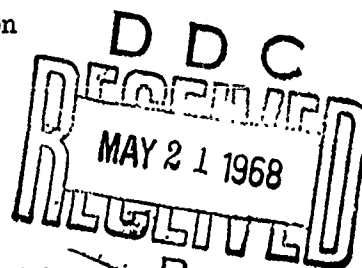
BY

W. A. MARTIN

SEPTEMBER 10, 1958

ENGINEERING DEPARTMENT

C O N V A I R
A Division of General Dynamics Corporation
(San Diego)



C O N T E N T S

	<u>Page</u>
TABLE OF CONTENTS	i
LIST OF ILLUSTRATIONS	ii
LIST OF TABLES	vi
SUMMARY	vii
1. INTRODUCTION	1
2. THE SIMPLE SHOCK TUBE	1
3. BASIC SHOCK TUBE EQUATIONS	3
4. MODIFICATION OF THE SIMPLE SHOCK TUBE FOR THE PRODUCTION OF STRONG SHOCK WAVES	
4.1 Introduction	7
4.2 Multiple Diaphragm Shock Tubes	8
4.3 Area Discontinuities	11
4.4 Combustion Drivers	14
5. DEVIATIONS FROM IDEAL FLUID THEORY	
5.1 Real Gas Effects	15
5.2 Shock Wave Attenuation	20
6. METHODS OF GENERATING HYPERSONIC FLOW	
6.1 Expansion Nozzles	22
6.2 Starting Problems	24
6.3 The Reflected Method	26
6.4 The Tailored-Interface Modification	27
6.5 Real Gas Effects in a Hypersonic Shock Tunnel	29
6.6 Reynolds Number and Stagnation Temperature Simulation	30
7. CONCLUDING REMARKS	31
REFERENCES	32
APPENDIX A.	36
ILLUSTRATIONS	38
TABLES	72

LIST OF ILLUSTRATIONS

	<u>Page</u>
Figure 1	
The wave system in the shock tube. The bottom half of the sketch indicates the pressure, temperature and Mach number at time, $t = t_1$	38
Figure 2	
Variation of shock pressure ratio, P_{21} with diaphragm pressure ratio, P_{41} , $\gamma = 1.4$.	39
Figure 3	
Variation of shock Mach number, M_s and particle velocity, U_{21} with diaphragm pressure ratio, P_{41} for $\gamma = 1.4$.	40
Figure 4	
The double diaphragm shock tube - reflected shock type	41
Figure 5	
The double diaphragm shock tube - unsteady expansion type	41
Figure 6	
Shock tube with an area discontinuity	42
Figure 7	
Shock tube with a convergent transition section	42
Figure 8	
Performance comparison of a variable geometry and simple shock tube, $\gamma = 1.4$.	43
Figure 9	
Performance of a hydrogen-air shock tube with an over-all pressure ratio of 10,000 showing the effects of varying the pressure and molecular weight of the buffer gas.	44

Figure 10

Performance comparison of various driver gases for $A_4/A_1 = 1$ and

$$A_4/A_1 = 6.25$$

45

Figure 11

Variation of temperature ratio, T_{21} with shock Mach number, M_S

46

Figure 12

Density ratio variation across the initial shock wave.

47

Figure 13

Variation of flow Mach number behind the initial shock wave

48

Figure 14

Attenuation of strong shock waves in slender shock tubes

49

Figure 15

Overall area ratio vs. flight Mach number ($\gamma = 1.4$, no reflection).

50

Figure 16

Wave diagram for a hypersonic shock tunnel

51

Figure 17

The Cornell Aeronautical Laboratory 11- by 15- inch hypersonic
shock tunnel

52

Figure 18

Pressure ratio across diaphragm vs. flight Mach number for
perfect starting (no reflection)

53

Figure 19

Pressure ratio across diaphragm vs. strength of reflected shock
($\gamma = 1.4$, no reflection)

54

Figure 20

Schematic drawing of hypersonic shock tunnel with plenum chamber

55

Figure 21

Ratio of pressure in low pressure section to plenum pressure vs.
flight Mach number for ideal gas ($\gamma = 1.4$, no reflection) 56

Figure 22

Wave diagram for the reflected shock 57

Figure 23

Pressure ratio across diaphragm vs. strength of reflected shock 58

Figure 24

Wave diagrams of shock tube modifications for increased testing
time 59

Figure 25a

Required diaphragm pressure ratio for tailoring at various flight
Mach numbers (unsteady configuration) 60

Figure 25b

Required diaphragm pressure ratio for tailoring at various flight
Mach numbers (steady configuration) 61

Figure 26a

Required initial driver gas temperature for tailoring at various
flight Mach numbers (unsteady configuration) 62

Figure 26b

Required initial driver gas temperature for tailoring at various
flight Mach numbers (steady configuration) 63

Figure 27

Variation of flight Mach number with shock Mach number with stagnation
enthalpy simulation 64

Figure 28a

Testing time for four modifications 65

Figure 28b

Nominal testing time of hypersonic shock tunnel modifications based
on equilibrium real gas calculations

66

Figure 29

Variation of test section Mach number with driver shock Mach number

67

Figure 30

Density in test section of hypersonic shock tunnel vs. test section
Mach number

68

Figure 31

Expansion of the hypersonic shock tunnel vs. test section Mach
number

69

Figure 32

Performance of the nonreflected method, $\gamma = 1.4$, $T_1 = 518.4^\circ\text{R}$, $T_f =$
 391.8°R , $R = 1716 \text{ FT}^2/\text{SEC}^2 \text{ }^\circ\text{R}$, $p_2 =$ static pressure behind the
incident shock (LB/IN^2)

70

Figure 33

Performance of the reflected method $T_1 = 518.4^\circ\text{R}$, $T_f = 391.8^\circ\text{R}$,
 $R = 1716 \text{ FT}^2/\text{SEC}^2 \text{ }^\circ\text{R}$, $p_6 =$ static pressure behind the reflected
shock (LB/IN^2)

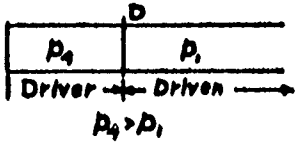
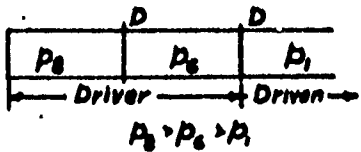
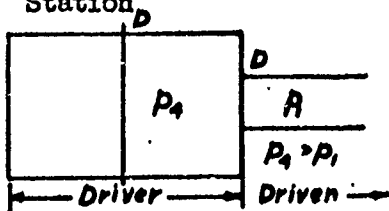
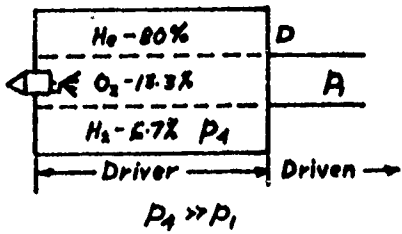
LIST OF TABLES

	<u>Page</u>
Table 1	
Flow quantities for very strong shock waves	72
Table 2	
Maximum shock Mach numbers for multiple diaphragm shock tubes	73
Table 3	
Maximum values of shock Mach number, M_s for $P_{41} \rightarrow \infty$	73

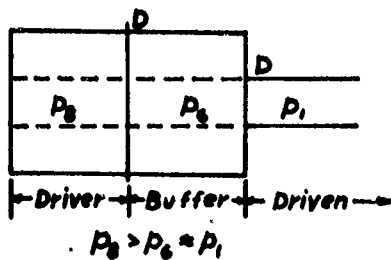
S U M M A R Y

A review has been made of the basic shock tube along with the various modifications required to produce hypersonic flow of short duration. Modifications to the driver system include multiple diaphragms, area discontinuities at the diaphragm station and combustion drivers. The influence of real gas effects, including shock wave attenuation, has been noted for both the production of strong shocks ($M_s > 3$) and the creation of hypersonic flow in an expansion nozzle. Nonreflected, reflected and tailored-interface type shock tunnels are discussed in Section 6 along with their starting problems, real gas effects and Reynolds number and stagnation temperature simulation. Detailed calculations have been omitted for simplicity but many figures have been presented which illustrate the operation of the various shock tube configurations. Further details may be obtained from the references given. The advantages and disadvantages of the various methods of producing hypersonic flow are summarized on the following pages.

DRIVER SYSTEMS FOR HYPERSONIC SHOCK TUNNELS

Type	Advantages	Disadvantages
1. Uniform Tube, Single Diaphragm Station 	1. Simplest method	1. Large diaphragm pressure ratio required to produce strong shocks.
2. Multiple Diaphragm Stations 	1. Overall pressure ratio reduced for a given shock Mach number or a gain in M_3 for a given $P_{4,1}$. 2. May be combined with buffer gas technique in order to use cold drivers.	1. Added complexity. Probably not too practical when more than two diaphragms are used.
3. Area Discontinuity at the Diaphragm Station 	1. Overall pressure ratio less than that of (1) for same conditions. 2. May be combined with (2) to give an additional gain in performance over (2).	1. Diaphragm pressure ratio required is still relatively high when used with cold drivers. 2. Driver section must be reinforced due to larger area.
4. Combustion Driver 	1. May be used for any of the above methods. 2. Increases both pressure and internal energy ratio across diaphragm. 3. Theoretically, most efficient form of driver	1. Added complexity of igniting driver gas. 2. May be erratic in operation-detonation is a problem. 3. Difficult to achieve constant volume burning which is most efficient combustion system. 4. Attenuation greater than cold drivers 5. Driver section must be reinforced to withstand increased pressure.

5. Buffer Gas



1. Enables cold hydrogen to be used as driver without creating combustion at the contact surface.

2. Reduced overall diaphragm pressure ratio for same shock Mach number or increased M_S for same overall P_{41} .

3. Combined with (3) to give performance equal to (4).

4. Attenuation problem alleviated.

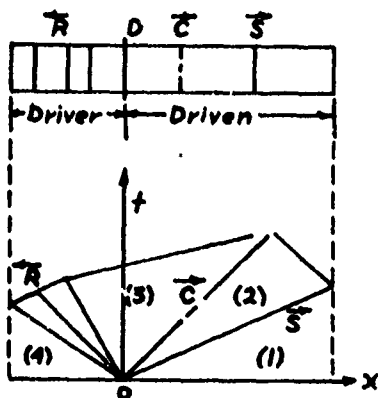
5. Extends range of tailored interface method for cold hydrogen driver to $M_S = 15$.

1. Added complexity of introducing a third gas.

2. Two diaphragm stations required.

HYPERSONIC TEST FACILITIESTypeAdvantagesDisadvantages

1. Simple Shock Tube



1. Simplest method.
2. Simulate Re and temperature without any modifications.

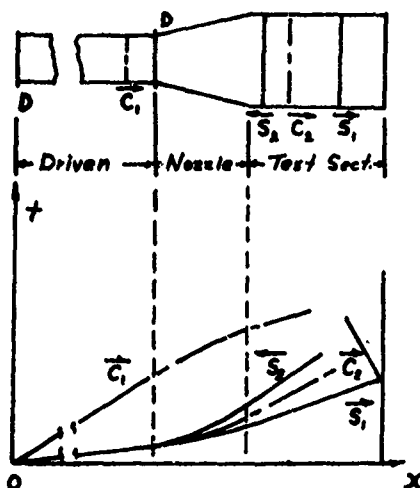
1. Maximum Mach number in test region is approximately three.

2. A long tube is needed to obtain a reasonable test time.

3. Attenuation problems.

4. Relatively small models.

2. Divergent Expansion Nozzle - Non-reflected Method



1. Larger models.
2. Increase in test Mach number for same shock Mach number.
3. May be added at exit of type 1 without modifying existing structure.

1. Moderate Re simulation.

2. Attenuation still a problem.

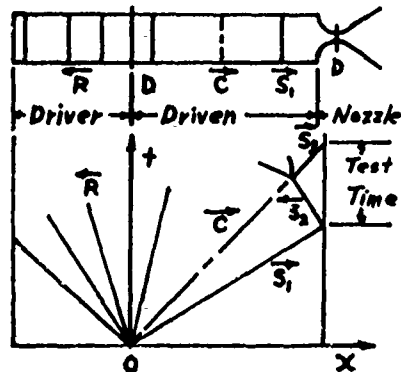
3. Tube must be as long as type 1.

4. Running time only slightly longer than type 1.

5. Starting problems may require the addition of a plenum chamber.

6. Two step nozzle may be required for hypersonic Mach numbers.

3. Reflected Method



1. Large models.
2. Higher test Mach number for same M_s than types 1 and 2.
3. Attenuation problem only affects production of reservoir conditions so smaller diameter tube may be used.
4. Slightly longer test time than types 1 and 2 for same test Mach number.

1. Low Re simulation

2. Tube still relatively long.

3. For same shock Mach number test time reduced due to reflected shock **interacting** with the contact surface.

TypeAdvantagesDisadvantages

3. (contd.)

5. Starting pressure ratio less than type 2

4. Stagnation temperature may be high enough to cause formation of nitric oxide which may be frozen by expansion.

4. Tailored-Interface Method - Unsteady Modification

1. Large Model.

1. Low Re as for type 3.

2. Same test Mach number range as type three.

2. Running times are long enough to cause erosion at nozzle throat.

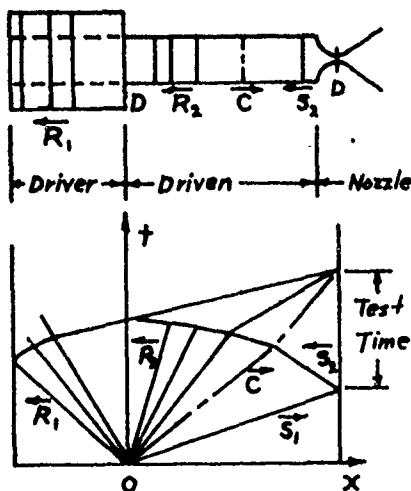
3. Test times nearly 8 times greater than type 2.

4. Channel length may be reduced.

3. Radiation losses may be important.

5. Attenuation less due to shorter channel.

4. Driver gas must be heated at higher Mach numbers in order to achieve tailoring (see also Page iv, -type 5.)



5. Longer driver section must be longer than for type 3.

6. Driven section must withstand higher pressure than types 2 and 3.

5. Tailored-Interface Method - Steady Modification

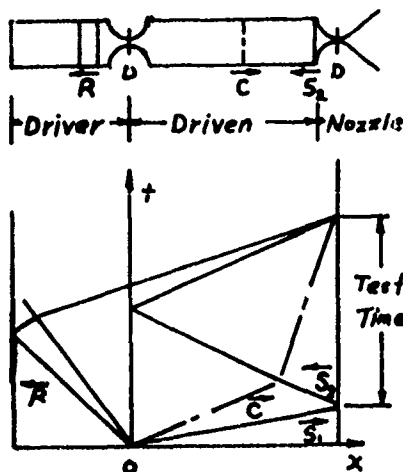
1. Test times are 25 times that of type 2.

1. Nozzle at diaphragm station must be changed for each test Mach number.

2. Other advantages as above.

2. Diaphragm pressure ratio is higher than type 4.

3. Other disadvantages as above.



1. INTRODUCTION

During the past five years the shock tube, and its various developments, have achieved prominence as a device for the study of hypersonic flow. This apparatus has an advantage over the wind tunnel in that both Mach number and temperature can be simulated. There is a disadvantage in that total testing times are very short, of the order of one millisecond, so that special instrumentation techniques are required for the measurement of the flow quantities. However, methods have been developed for physical measurements in the short time available and quite acceptable results have been obtained.

It is the purpose of this report to outline some of the more recent developments of the shock tube principle. As these developments are only modifications, a brief resume of the theory and operation of the simple shock tube will also be presented. A more historical introduction is to be found in Refs. 1, and 2 which contain many references to earlier research in this field. A review of more recent advances is given by Hertzberg (Ref. 3) and Glass and Hall (Ref. 4).

2. THE SIMPLE SHOCK TUBE

The simple shock tube consists of a straight tube of uniform cross-section separated by a thin diaphragm which divides the tube into two compartments and enables a pressure ratio to be created between them. One compartment is known as the high pressure chamber, or driver section, the other, the low pressure channel, or driven section. Usually the driver section is pressurized while the driven section may be either

evacuated or at atmospheric pressure. The gases in both sections are normally in thermal equilibrium. Upon rupturing the diaphragm the wave system shown in Fig. 1 is established.

Theoretically, upon removal of the diaphragm, a shock wave is propagated into the low pressure section and the high pressure gas expands into the driven section by means of a rarefaction wave centered at the origin. This is not quite true in practice as the rarefaction wave is not centered at the origin and the shock wave takes a finite time to form from a series of compression waves created when the diaphragm is removed. However, these deviations from the ideal theory are not too important for practical purposes and after the shock has formed it is considered to travel at a constant velocity.

The gas in the driven section is compressed and heated by the shock wave while the driver gas is expanded and cooled by the rarefaction wave. Thus two bodies of gas exist in the shock tube which are brought to the same pressure and have the same particle velocity but due to different formative processes their temperature, density and entropy are different. These two states are separated by an interface or contact surface which in practice is more of a region rather than a plane surface. This contact surface, or contact front as it is called by some authors, travels at the particle velocity. Therefore, behind the shock there is a region of steady flow at a high pressure and temperature while behind the contact surface the flow is again steady with the same pressure but at a lower temperature. Due to the steady

nature of these states many attempts have been made to utilize them for aerodynamic testing. The particle velocities are identical in each state but due to the lower temperature in (3) the Mach number (M_3) is higher than in (2). However, state (2) is more adaptable to hypersonic testing due to temperature requirements and in practice is found to be much more uniform than region (3). (5) (6) (7) The testing time is determined by the length of the driver and driven sections, the gas combination used and the strength of the initial shock wave. (2) If the shock tube is too short the flow will be terminated very quickly by reflected waves from the closed ends. For an infinitely long tube the test time at a station, x is the interval between the arrival of the initial shock wave and the passing of the contact surface. Therefore, for strong shocks, where the contact surface velocity is high, the test section should be as far as possible from the diaphragm station. The total lengths of the driver and driven sections must be chosen so that the reflected shock and rarefaction waves do not return before the arrival of the contact surface. The ideal lengths will be such that the reflected shock and rarefaction meet the contact surface at the test section.

3. BASIC SHOCK TUBE EQUATIONS

The states on each side of the rarefaction are related by the isentropic relationships while the normal shock relationships are employed for the transition across the shock front. These two solutions

can be matched at the contact surface and the physical properties of the complete shock tube flow determined. This procedure leads to the following identity which is the basic equation for the shock tube.

$$P_{14} = \frac{1}{P_{21}} \left[1 - (P_{21} - 1) \sqrt{\frac{\beta_4 E_{14}}{\alpha_1 P_{21} + 1}} \right]^{\frac{1}{\beta_4}} \quad (3:1)$$

Equation (3:1) indicates that the shock pressure ratio (P_{21}) is a function of the diaphragm pressure ratio (P_{14}), the internal energy ratio (E_{14}) and the specific heat ratio of the driver and driven gases (γ_4 and γ_1). The requirements for producing strong shock waves, which are necessary in order to achieve temperatures suitable for hypersonic simulation, may be better examined by allowing the diaphragm pressure ratio, (P_{14}) to equal zero in the above equation. This gives the following:

$$(P_{21})_{P_{14}=0} = 1 + \frac{\alpha_1}{2\beta_4 E_{14}} + \sqrt{\frac{1}{\beta_4 \beta_1 E_{14}} + \left(\frac{\alpha_1}{2\beta_4 E_{14}} \right)^2} \quad (3:2)$$

Upon examination of this equation it is found that two methods present themselves for the production of strong shock waves in a simple shock tube. The diaphragm pressure ratio, (P_{14}) can be made very large or the energy ratio across the diaphragm, (E_{14}) can be made very small, or both. The energy ratio may be reduced by heating the driver and cooling the driven gases, but a more common method is to use a light driver gas and a heavy driven gas. The aerodynamicist usually likes to use

air as a test gas, with possibly nitrogen as a second choice, with helium or hydrogen drivers. Figure 2 gives the diaphragm pressure ratio required for a range of shock pressure ratios for the combination Air/Air, He/Air, and H_2 /Air for the simple shock tube case while Fig. 3 presents the variation of shock wave Mach number, (M_s) and particle velocity, (U_{21}) with diaphragm pressure ratio, (P_{h1}) for the three gas combinations.

It can be seen from these two figures that a great advantage is gained by the use of helium or hydrogen as a driver gas. The internal energy ratio can also be reduced by heating the driver gas either by electrical heating or by the ignition of combustible mixtures which give high values of T_4 . The combustible mixture is usually a stoichiometric mixture of hydrogen and oxygen diluted with excess hydrogen or helium.⁽⁸⁾ This method has seen widespread use for the production of strong shock waves in shock tubes. Another method used in gun tunnel versions of the shock tube is to compress the driver gas by a piston driven by an explosive process, usually the ignition of a powder charge. This compression raises the pressure and temperature to a predetermined level governed by the strength of the diaphragm which then bursts initiating the flow.

Having established Eq. (3:1) all the other flow quantities can be determined. The most useful equations are listed below in nondimensional notation. ⁽²⁾

1. Density ratios

$$\Gamma_{34} = P_{34}^{\gamma_4} = [P_{14} P_{21}]^{\gamma_4} \quad (3:3)$$

$$\Gamma_{21} = \frac{1 + \alpha_1 P_{21}}{\alpha_1 + P_{21}} \quad (3:4)$$

2. Speed of sound and temperature ratio

$$A_{34} = T_{34}^{\frac{k}{2}} = P_{34}^{\beta_4} = [P_{14} P_{21}]^{\beta_4} \quad (3:5)$$

$$A_{21} = T_{21}^{\frac{k}{2}} = \left[\frac{P_{21} (\alpha_1 + P_{21})}{1 + \alpha_1 P_{21}} \right]^{\frac{1}{2}} \quad (3:6)$$

3. Velocity of the shock wave

$$M_s = [\beta_1 (1 + \alpha_1 P_{21})]^{\frac{1}{2}} \quad (3:7)$$

4. Particle velocity or contact surface velocity

$$U_{21} = \frac{P_{21} - 1}{\gamma_1 [\beta_1 (\alpha_1 P_{21} + 1)]^{\frac{1}{2}}} \quad (3:8)$$

$$U_{34} = \frac{1}{\gamma_4 \beta_4} [1 - (P_{14} P_{21})^{\beta_4}] = A_{14} U_{21} \quad (3:9)$$

5. Local Mach numbers

$$M_3 = \frac{U_{34}}{A_{34}} = \frac{1}{\beta_4 \gamma_4} [(P_{14} P_{21})^{-\beta_4} - 1] \quad (3:10)$$

$$M_2 = \frac{U_{21}}{A_{21}} = \frac{P_{21} - 1}{\gamma_1 [\beta_1 P_{21} (\alpha_1 + P_{21})]^{\frac{1}{2}}} \quad (3:11)$$

6. Speed of the head and tail of the rarefaction wave

$$C_{34} = U_{34} - A_{34} \quad (3:12)$$

$$C_{44} = -1$$

The head of the rarefaction wave travels at the velocity of sound of the driver gas.

It is of interest to examine the limits of these equations for an infinite value of the diaphragm pressure ratio. Table I is a comparison of three different driver gases, air, helium, and hydrogen in combination with air as a driver gas. Table I indicates more than a ten-fold increase in shock strength when hydrogen, rather than air, is used as a driver gas. This same increase is obtained in the temperature achieved in the region behind the shock, however, the Mach number in the steady state region (2) is limited by this temperature increase, and even for the ultimate case, where P_{14} and E_{14} are both zero, the limiting Mach number (M_2) is only 1.89. Thus Table I illustrates that although high temperatures may be achieved this Mach number restriction prevents true hypersonic simulation in a simple shock tube. The results shown in Table I are based on perfect gas theory (i.e. $\gamma = 1.4$) which does not hold for the extreme shock pressure ratios calculated.

4. MODIFICATION OF THE SIMPLE SHOCK TUBE FOR THE PRODUCTION OF STRONG SHOCK WAVES

4.1 INTRODUCTION

It is possible to improve the performance of the simple shock tube by suitable modifications. These modifications include the installation

or additional diaphragm stations and driver sections whose cross-sectional area is greater than the driven section. (9) (10) (11) The former method is a device which sacrifices pressure ratio in favor of an increased temperature ratio. The latter creates an additional expansion at the diaphragm station which converts thermal energy into kinetic energy. Therefore, in both cases, it is possible to produce the same shock strength as a uniform tube but with a smaller diaphragm pressure ratio, or conversely, to produce a stronger shock for the same diaphragm pressure ratio. Another method, which increases the temperature ratio across the diaphragm, is to use a combustible mixture as a driver gas. Rather than use combustible mixtures it is sometimes more satisfactory to use either cold helium or hydrogen as a driver, as mentioned in Section (3). A further modification of this technique has been to introduce an inert buffer gas between the hydrogen driver and the air test gas with an area discontinuity at the buffer-air diaphragm station. (12) (13) These methods will now be examined in more detail.

4.2 MULTIPLE DIAPHRAGM SHOCK TUBES

Figure 4 is a sketch of a shock tube of constant area utilizing two diaphragms. D_1 is the primary diaphragm which is ruptured first producing the shock S_6 . This shock wave is reflected at diaphragm D_2 bringing the gas in state 5 to rest and raising its temperature and pressure. After a short delay, diaphragm D_2 is removed and a new wave system is produced resulting in the shock wave S_1 which is of greater strength than the shock, S_6 . Comparing Fig. 1 and Fig. 4 for the same overall temperature and pressure, and with $T_1 = T_6 = T_8$, $\gamma_1 = \gamma_6 = \gamma_8$,

will give an idea of the increase in shock strength for the double diaphragm case. As the gas is brought to rest ahead of D_2 the pressure and temperature ratios of interest in both cases are P_{41} and T_{41} . However, $P_{4d} < P_{4s}$ while $T_{4d} > T_{4s}$ which gives a shock of greater strength than the system shown in Fig. 1. As an example of the gain to be expected by the addition of diaphragm D_2 consider the case where the overall pressure ratios, P_{41} (Fig. 1) and P_{81} (Fig. 4) are both equal to 10^3 . Then from the Air/Air curve of Fig. 3, $M_s = 3.14$. For the case shown in Fig. 4 let $P_{61} = 10$ which means $P_{86} = 10^2$. The initial shock wave Mach number, M_{s6} will be found using Fig. 3 and is 2.37. The final overall pressure ratio will be $P_{41} = P_{46} \times P_{61}$. The value of P_{46} is obtained from interpolation of Table III in Ref. (9) ($P_{46} = 25.85$) while $T_{46} = 3.236$. Having determined these new initial conditions, the final shock Mach number, $M_s (=3.77)$ can be obtained by interpolation from Table I Ref. (9). It is seen that a gain of 20% in shock Mach number is obtained by the addition of the diaphragm, D_2 . The intermediate pressure, P_6 can be adjusted so as to give a maximum shock Mach number for a given overall pressure ratio, P_{81} .

The above method may be somewhat simplified by making D_2 weak enough that the initial shock wave, M_{s6} will rupture it on contact. This produces an unsteady expansion from state 6 to state 1 resulting in a less efficient process than the reflected shock type described above, but reducing the complexity of the system caused by the introduction of a mechanical or electrical delay. The wave diagram for this type of shock tube is shown

in Fig. 5. The analysis for this case is carried out in Ref. 9.

Carrying out the same calculation for the same conditions as used for the example of the reflected shock type of double diaphragm shock tube gives a final Mach number, M_{S1} of 3.73 which is only a decrease of approximately one percent. This variation would be larger at higher Mach numbers but the percentage decrease would probably never be large enough to warrant adopting the delay type installation for a straight shock tube.

Ref. 9 indicates that for the maximum gain in M_s the pressure must be approximately the geometric mean of the pressures on either side. Then for a multiple diaphragm shock tube the overall pressure ratio is given by $P_0 = P_1^n$, where P_1 is the individual pressure ratio across each diaphragm and n is the number of diaphragms. It can be shown (Ref. 9) that there is a maximum shock Mach number attainable irrespective of the number of diaphragms used and depending only on the overall pressure ratio, across the shock tube. This relationship is $M_s \text{ Max.} = P_0^{3/14}$ and Table II gives the values of $M_s \text{ Max.}$ attainable over a range of reasonable overall pressure ratios for the conditions of equal γ and T throughout. It is also shown in Ref. 9 that a multiple diaphragm system, where all the diaphragms except the first have zero pressure difference across them, is another method for creating strong shock waves. If a shock wave of Mach number greater than 2.67 is generated by rupturing the first diaphragm then, theoretically, the maximum obtainable shock speed increases without limit. In this system the shock wave reflecting off each successive diaphragm will increase

the pressure and temperature ahead of that diaphragm producing a successively stronger shock.

4.3 AREA DISCONTINUITIES

As outlined in Section 2 the basic shock tube comprises a driver and driven section of uniform cross-section separated by a diaphragm. However, many authors have shown that there is a gain in the final shock strength by introducing an area discontinuity at the diaphragm station. This arrangement may also be combined with the double diaphragm method to give a further increase in the final shock strength. This latter method is illustrated in Fig. 6. The area change may also be accomplished by a transition section as shown in Fig. 7.

In Fig. 6 if diaphragm D_2 is eliminated a single shock system is set up at D_1 , with S_5 being replaced by a rarefaction wave as in the case of a uniform tube. If the shock S_1 , is such that $M_3 < 1$ then the wave system will be as shown in Fig. 1, the flow being accelerated subsonically to M_3 . However, if $M_3 > 1$ the gas in (6) is accelerated to sonic velocity at the diaphragm station and is then further expanded by a rarefaction wave to the supersonic Mach number, M_3 . The addition of the diaphragm, D_2 combines the multiple diaphragm and variable geometry type using a convergent transition section which may or may not contain a convergent - divergent nozzle. However, the only advantage here is a smoother flow from the driver to the driven section as the flow processes are the same whether the area change is gradual or discontinuous.

As in the previous section a comparison will be made between the uniform and the variable geometry shock tubes by determination of the final shock Mach number achieved for identical overall pressure ratios. An analytical expression for such a gain factor is not possible but by use of tables and graphs it is possible to determine these values of \tilde{M}_{s1} . We will only consider the case of $M_3 > 1$ which corresponds to the range of shock strength required for hypersonic testing. Consider first the case where the diaphragm, D_2 is not present and that $A_{3b} = A_1$ is the minimum section such as shown in Fig. 7. Reference (10) develops the following expression for the overall pressure ratio, P_{41} .

$$P_{41} = \frac{P_{21}}{9} \left[1 + \frac{\gamma_4 - 1}{2} M_3^2 \right]^{\frac{2\gamma_4}{\gamma_4 - 1}} = \frac{P_{21}}{9} \left[1 - \frac{u_2}{a_1} \frac{a_1}{a_4} \frac{\gamma_4 - 1}{2} g^{\frac{-(\gamma_4 - 1)}{2\gamma_4}} \right]^{-\frac{2\gamma_4}{\gamma_4 - 1}} \quad (4:3:1)$$

where g is an equivalence factor given by

$$g = \left\{ \left[\frac{2 + (\gamma_4 - 1) M_{3a}^2}{2 + (\gamma_4 - 1) M_{3b}^2} \right]^{\frac{1}{2}} \left[\frac{2 + (\gamma_4 - 1) M_{3b}^2}{2 + (\gamma_4 - 1) M_{3a}^2} \right] \right\}^{\frac{2\gamma_4}{\gamma_4 - 1}} \quad (4:3:2)$$

As A_{3b} is the minimum section, M_{3b} will be equal to unity but M_{3a} must be determined in order to calculate g . Knowing the area ratio, A_4/A_1 then M_{3a} is determined from the following relationship.

$$\frac{A_4}{A_1} = \frac{M_{3b}}{M_{3a}} \left[\frac{2 + (\gamma_4 - 1) M_{3a}^2}{2 + (\gamma_4 - 1) M_{3b}^2} \right]^{\frac{\gamma_4 + 1}{2(\gamma_4 - 1)}} \quad (4:3:3)$$

It is seen from Eqs. (4:3:2) and (4:3:3) that for a given area ratio g is a constant when $M_3 > 1$. Therefore knowing the area ratio, g can be determined and a plot of P_{41} vs. P_{21} can be obtained. A comparison of the shock Mach numbers attainable for area ratios of 1, and ∞ is presented in Fig. 8. Table 3 is taken from Ref. (10) and gives the maximum shock Mach numbers when $P_{41} \rightarrow \infty$ for various gas combinations, four area ratios and two temperature ratio. Both Fig. 8 and Table 3 illustrate that the gain in shock strength is not too great even when the area ratio is infinite. Once again, however, the gain achieved by increasing the sound speed in the driver gas is indicated by Table 3.

As an example of the gain to be expected, through the use of an area change at the diaphragm, consider the example used previously. In this instance the area ratio will be 3:1, the diaphragm pressure, $P_{41} = 10^3$ for an Air/Air combination with a constant initial temperature ratio, T_{41} , which gives a final shock Mach number of 3.35. Combining the multiple diaphragm method (two diaphragms) with the same area discontinuity and total pressure ratio and with P_{86} (Fig. 6) $= 10^2$ gives $M_8 = 3.9$. This is an increase of 16 per cent due to the addition of D_2 to the system, and an increase of nearly 25 per cent over a simple shock tube with the same P_{41} .

The above example is for an air driver but we have seen from Fig. 3, and Tables 1 and 3, that a light gas such as hydrogen or helium is a more efficient driver. However, when hydrogen is used to produce shocks combustion occurs at the driver-driven interface which sets up severe

flow disturbances. Helium could be substituted as a driver but it is not as efficient. A method to eliminate this combustion problem is the use of a double-diaphragm shock tube with an inert buffer gas between the driving hydrogen and the driven air. There is also an area change incorporated at the diaphragm separating the buffer gas and the air. Figure 9 shows the effect of varying the pressure and molecular weight in various buffer gases for an overall pressure ratio of 10^4 . It is seen from the figure that a shock Mach number of approximately 15 can be obtained by the use of any of the inert gases given on the figure, however, the lighter gases such as helium require a large pressure ratio across the downstream diaphragm. Consider as an example a shock tube of this type with argon as the buffer gas. In order to produce a shock Mach number of 13 a simple shock tube using hydrogen as a driver would require a P_{41} of 7×10^4 . If a large area discontinuity is introduced the diaphragm pressure ratio is reduced to 1.8×10^4 . When an argon buffer is introduced between the driver hydrogen and driven gas an overall pressure ratio of only 3.5×10^3 is required which is a reduction by a factor of 20. This method seems to offer very good possibilities of producing strong shock waves using cold driver gases.

4.4 COMBUSTION DRIVERS

A common method of producing strong shock waves is by using a combustible mixture which is ignited to give high pressures and temperatures in the driver. A typical composition for a combustible driver is 13.33 per cent hydrogen 6.67 per cent oxygen and 80 per cent helium as a diluent. The ignition of the hydrogen and oxygen raises the

temperature and pressure of the helium which gives a large increase in the energy and pressure ratios across the diaphragm. Excess hydrogen has also been used as a diluent. Using this type of driver the diaphragm is usually burst by the combustion of the mixture. Combustion may be produced in three ways. A spark plug, or plugs, may be inserted in the driver section which is fed by a high voltage coil, producing the spark which causes ignition. A heating wire may be inserted the length of the high pressure chamber and a large current passed through it which causes a constant volume burning. The mixture may be allowed to ignite itself by introducing the combustible gases and then adding the diluent until the diaphragm ruptures, whereupon the hydrogen-oxygen mixture will ignite. It has been found that the constant volume process is the most efficient. There is also a practical limit to which the driver gas can be heated due to molecular dissociation at the higher temperatures. Figure 10 compares the theoretical shock Mach numbers obtained over a range of diaphragm pressure ratios for helium, hydrogen and combustion drivers. Curves are presented for both the simple shock tube, ($A_2/A_1=1$) and one where $A_2/A_1=6.25$.

5. DEVIATIONS FROM IDEAL FLUID THEORY

5.1 REAL GAS EFFECTS

In the previous chapters the discussions and calculations have been carried out assuming that the specific heat ratio, γ remained constant. However, for shock Mach numbers greater than three the temperatures produced are high enough to invalidate this assumption and the variations from an ideal gas must be considered. (14) (15) Above $M_s = 3$ fairly high temperatures will be achieved in state (2) and very low temperatures in

state (3). For an M_s of 4.0, with an Air/Air combination, the temperature T_3 will be 40°K which is below the boiling point of nitrogen and oxygen. In state (2) the temperature, T_2 will be over 1200°K on the basis of the ideal theory. At these temperatures the specific heat ratio, can no longer be taken as 1.4 and above $M_3 = 3$ the gas can no longer be considered an ideal fluid and the real gas effects must be considered.

We are concerned primarily with state (2) behind the shock, as this will be our test gas, so our discussion will be limited to this region. The internal energy content of a diatomic gas is made up as follows:

- 1) The kinetic energy of translation of a molecule
- 2) The energy of molecular rotation
- 3) The energy of molecular vibration
- 4) The energy of molecular dissociation into atomic groups
- 5) The energy of electronic excitation
- 6) The energy of ionization

As the temperature is increased the higher rotational and vibrational levels are excited absorbing heat in the process. This causes an increase in the heat capacity which in turn increases the specific heats, C_p and C_v . However, as they both increase about the same amount then the ratio, γ will be smaller. Added to this effect the specific heats, and the molecular weight, become pressure dependent. Above 2000 - 3000°K dissociation occurs giving nitrogen, oxygen and their atomic states. These temperatures are also high enough to cause

chemical reactions such as the formation of nitric oxides. At still higher temperatures ($\sim 6000^\circ\text{K}$) electronic excitation and ionization occur and the air becomes almost completely dissociated giving atomic oxygen and nitrogen as before, small percentages of the various oxides of nitrogen, electrons, negative O_2 ions and positive ions of nitric oxide. These conditions would be the same as those produced at the stagnation point of an insulated blunt body traveling at Mach number of 16 at an altitude of 60,000 feet.

The transition through a strong shock wave can be qualitatively described as follows. At the shock front the temperature jumps to a high value as active degrees of freedom, translation and rotation are excited almost immediately in the distance of a few mean free paths. After this initial jump thermal equilibrium will be reached in an exponential manner as energy is transferred to the remaining degrees of freedom during the relaxation period. Therefore, besides the variation in the flow properties, some consideration must be given to the relaxation time to insure that equilibrium conditions exist for the test to be performed.

Figure 11 indicates the variation of the temperature T_2 with shock Mach number, M_3 for two values of the initial pressure. It is seen that the real gas temperatures are lower at the higher Mach numbers as expected from the preceding discussion. Figure 12 compares the density ratio for a real and an ideal gas over the same range of M_3 as used in Fig. 11. Here the real gas density is higher than the

ideal gas case which approaches a limit of 6 while at $M_g = 12$ the real gas density ratio continues to increase. Due to the increase of density and decrease of temperature the pressure is found to be very near the same for the real gas as for the ideal gas. Therefore, Equation 3.1 will give a fairly good approximation for real gas calculations.

The decrease in temperature behind the normal shock in a real gas is more pronounced than the change in specific heat ratio or the decrease in molecular weight. Therefore, the speed of sound in a real gas is lower for the same shock strength than for the ideal case giving a higher attainable Mach number, M_2 behind the shock. This is illustrated in Fig. 13. The maximum value of M_2 for the ideal case is 1.89 but Fig. 13 indicates that an $M_2 > 3$ can be obtained for a real gas. As the Mach number of the flow in region (2) is increased while the temperature and speed of sound are decreased then the particle velocity must be changed very little by the real gas effects. This is found to be the case with the real values of U_2 being only slightly greater than the ideal value.

The real gas curves shown in Figs. 11, 12 and 13 were computed using the charts and tables contained in references 18 and 22. The crossover of the two real gas curves in Fig. 13 is due to the identical behaviour of the speed of sound ratio with increasing temperature. The ideal gas curves were computed from Equations 3.4, 3.6 and 3.11. References 18 and 22 are two examples of the many excellent sets of tables and graphs available for the determination of the flow properties behind strong shock waves. (16-23)

Table III indicated that there was no appreciable gain in performance by introducing an area change at the diaphragm station. However, these calculations were based on the driver gas being ideal. It has been shown that if the driver gas density is increased to a very high value then there is a considerable gain in performance by using a large driver-driven area ratio.⁽²⁴⁾ This difference is due to the behaviour of the attractive and repulsive intermolecular forces. At normal densities these forces are negligible and the performance of a uniform and non-uniform tube are nearly identical. However, if the driver density is increased to a very high value there is a considerable advantage in increasing the chamber area as the repulsive forces then predominate. It was found in Ref. 24 that an area ratio of five was nearly equivalent to an infinite area ratio, while a chamber twice the area of the channel would give half the performance promised by the infinite value for the case of nitrogen and hydrogen drivers at pressures of 6000 and 2200 atmospheres respectively. It was found that at intermediate densities the performance relative to an ideal gas would be almost the same for the non-uniform tube and considerably reduced for the uniform tube. The test time for identical length chambers is reduced when using high density drivers due to the increase in sound speed, a_d , which means that the rarefaction waves reflected from the end at the high pressure section will travel at a higher velocity. Increasing the chamber length would recover this loss in test time.

5.2 SHOCK WAVE ATTENUATION

The ideal shock tube theory predicts that when the diaphragm breaks a flow will be set up as shown in Fig. 1. According to this theory a plane shock wave is produced which travels down the tube at a constant velocity followed by two steady states separated by a contact surface. In practice however, this model is not realized. (2) Instead the shock wave velocity is found to decrease with distance from the diaphragm. In fact the shock does not reach its calculated speed until a short distance from the diaphragm due to the formation process. The shock only attains the ideal value for weak shocks, for as the diaphragm pressure is increased the shock never reaches the theoretically predicted speed, rising to a maximum some distance from the diaphragm and then attenuating as it progresses down the tube. This effect is also more pronounced as the shock tube diameter is decreased.

Due to this shock attenuation, the flow quantities in states (2) and (3) are not steady but vary with time as the shock progresses down the tube thereby making testing in these regions very difficult. The problem of shock attenuation has received a great deal of attention in the last five years. (25 - 28) Many of these investigators have focussed their **attention** on the viscous effects which, of course, are not allowed in the ideal theory. There have been studies made of the boundary layer both theoretical and experimental to determine the causes of the attenuation. (29,30-32) A satisfactory explanation has not been arrived at although the theories of Trimpf and Cohen and Kirels and Braun give good agreement at lower Mach numbers. There is probably some influence of the diaphragm station especially at the higher shock strengths where

metal diaphragms are used and take a finite time to open. This effect may be instrumental in reducing the velocity U_3 which must match U_2 at the contact surface. The complete flow can be considered to be governed by conditions at the contact surface therefore a reduction in the velocity U_2 will produce a reduction in the shock speed.

The detailed processes of attenuation are not too important in the operation of a shock tunnel but it is desirable to have as little attenuation as possible so that the flow conditions will be fairly steady during the test period. Considerable work has been carried out to determine what initial conditions will give the least attenuation. (28,33) In addition to the causes given above it has been generally found that a greater attenuation is experienced as the sound speed of the driver gas is increased. Figure 14 shows typical attenuation measurements for several driver gas compositions. The results for helium give the least attenuation but this driver gives the lowest initial shock strength. The combustion driver, which is the most efficient type, produces the highest initial shock strength but at L/D of 150 the shock has attenuated to a lower speed than the helium driven shock. It is necessary in both straight shock tubes and non-reflected type shock tunnels to have as long a driver section as possible in order to have reasonable test times. The attenuation could be alleviated by increasing the diameter thus reducing the L/D ratio but there is a limit to this due to structural and handling reasons.

Experimental evidence has shown that the attenuation is inversely proportional to the shock tube Reynolds number, $(a_1 D_1 / \nu_1)$. For a given shock tube using air as the test gas the Reynolds number can

only be adjusted through the kinematic viscosity or more precisely by adjusting the initial pressure, p_1 . From the attenuation standpoint, it is desirable to have p_1 as large as possible. However, if cold drivers are used, which seems desirable from a study of Figure 14, a low initial pressure will be required to produce the diaphragm pressure ratio to give the same shock strength. These requirements are at cross purposes and, as usual, a suitable compromise must be found in order to reduce the attenuation effects.

6. METHODS OF GENERATING HYPERSONIC FLOW

6.1 EXPANSION NOZZLES

It has been shown in the previous section that, although the proper temperature may be achieved in a straight shock tube, the maximum Mach number is too low for hypersonic simulation. In order to overcome this difficulty the hypersonic shock tunnel was developed. By placing an expansion nozzle at the downstream end of the conventional shock tube the flow behind the shock can be expanded to a higher Mach number.⁽³⁴⁻³⁷⁾ Therefore, by a proper choice of shock strength and expansion ratio it is possible to simulate both temperature and Mach number. Figure 15 presents the shock tube area ratio required over a range of test section Mach numbers.

The simplest type of installation is a single stage expansion nozzle placed at the exit of the driven section of the tube, the final Mach number being determined by the area ratio. This system is known as the nonreflected method. In Ref. (35) a set of mahogany liners were installed in the shock tube with the nozzle located at the

existing test section. Using this simple scheme a study was made of the flow in the nozzle. Figure 16 illustrates the wave system set up in a shock tube of this type. As the initial shock wave, S_1 enters the nozzle it weakens locally and develops curvature which propagates from the wall to the centerline of the tube as the shock moves into the test section. As the shock weakens the velocity of the particles behind decreases, however, the particles originally set in motion by the passage of the shock down the uniform tube, (A_6) accelerate as they pass through the expansion waves at the mouth of the nozzle and increase in velocity. Therefore, there is another shock created which separates the two flow regions 2 and 4, (Fig. 16). Due to the entropy being different behind each shock there is also a contact surface formed which separates the regions 2 and 3, (Fig. 16). The wave S_2 attempts to propagate upstream but as it is moving against a supersonic flow it is swept downstream through the nozzle. As S_1 moves through the nozzle it weakens which, in turn, causes S_2 to become stronger. If S_2 grows sufficiently strong it will not be swept out of the nozzle but will remain standing in the nozzle preventing the tunnel from starting.

Shock tunnels have been built which use double and triple expansion nozzles for the generation of hypersonic flow. This system enables the test section area to be reduced over that required for the system shown in Fig. 16. In order to obtain reasonable testing times at hypersonic Mach numbers it is necessary to have a fairly long shock tube. However, with long tubes the boundary layer built up on the walls may be quite

thick causing severe attenuation problems. A method of circumventing this is to increase the diameter but this in turn means increasing the test section area of the driven section. By introducing a two step nozzle, which gives two stage expansion and also drains off the boundary layer created behind the initial shock wave, the test section area can be decreased. This type of shock tunnel is illustrated in Fig. 17.

6.2 STARTING PROBLEMS

The flow duration is the time between the departure of the starting wave system S_1 , C_2 , S_2 , Fig. 16, from the test section and the arrival of the initial contact surface. In order to make this testing time as long as possible it is necessary to ensure that this wave system is swept through the test section in as short a time as possible.⁽³⁸⁾ The governing factor is the strength of S_2 which for ideal starting must be a sound wave. By placing a diaphragm at the nozzle entrance the test section can be evacuated to a pressure much below the pressure in the uniform tube which will in turn strengthen the initial shock wave when it enters the nozzle. Therefore the velocity difference across S_2 will be reduced and in the limit S_2 will become a sound wave. If the initial pressure in the nozzle is decreased still further expansion waves will be formed moving towards the nozzle entrance. However since expansion waves move at the local speed of sound relative to the flow there is no gain in reducing the pressure ratio across the nozzle diaphragm below that value required to make S_2 a sound wave. Fig. 18 gives the pressure ratio required across the nozzle diaphragm to ensure perfect starting for a range of test section Mach numbers. This figure

indicates that an extremely large pressure ratio is required to obtain a perfect start for Mach numbers greater than 10.

Figure 19 shows the effect of reducing the pressure ratio across the nozzle diaphragm thus giving an imperfect start. In this case the wave S_2 (Fig. 16) will stand in the nozzle and suggests the possibility of placing a plenum chamber downstream of the test section. This chamber will create an expansion wave which will then move upstream, weaken the shock S_2 and pull it through the test section. A schematic drawing of the arrangement is shown in Fig. 20 while Fig. 21 indicates the pressure ratio required of the plenum chamber for a range of hypersonic Mach numbers in the test section.

A plenum chamber may also be employed when the shock S_2 is not standing in the test section. In this case the expansion waves from the plenum will further accelerate the starting process and thus increase the test time. If the pressure in the nozzle and test section were low enough to ensure a perfect start, addition of a plenum chamber would not improve starting, however, the addition of a plenum is advantageous in another way. For a perfect start, S_1 (Fig. 16) passes through the test section at a high velocity and a long test section is required to prevent the reflected wave returning and destroying the flow before the arrival of the original contact surface, C_1 . By adding a plenum chamber at the end of the test section this reflected shock can be greatly weakened. Therefore, by using a plenum of large cross-sectional area and shock length the facility may be made more compact and even reduce the pumping capacity required.

6.3 THE REFLECTED METHOD

If, instead of the straight expansion nozzle, the driven section is terminated by a regular convergent-divergent hypersonic nozzle a reflected type shock tunnel results. At the hypersonic Mach numbers of interest the area ratio is so large and the throat area so small that the nozzle will act as a solid plate and the initial shock wave will be completely reflected. This means that the gas following the shock will be compressed a second time and brought to rest creating a high pressure, high temperature, stagnant reservoir of air to be expanded through the nozzle. The reflected shock governs the duration of steady flow, interacting with the contact surface and returning to the nozzle. A wave diagram and sketch of this method is shown in Fig. 22.

The reflected method has the advantage that hypersonic flow is initiated from a reservoir with almost constant supply conditions. Therefore, the problems of shock attenuation, which would constantly vary the test conditions, and boundary layer build up behind the initial shock wave are not present. For the same temperature requirements the initial shock may be weaker than in the nonreflected case, or conversely, higher stagnation temperatures are obtained for the same shock strength. The testing time for the same Mach number is also slightly increased due to the decrease in required initial shock strength.

The starting problems with this type of tunnel are essentially the same as that of the nonreflected type and a diaphragm at the nozzle is

desirable in order to reduce the starting time. In the nonreflected case the entrance Mach number may be as high as 1.89, based on perfect fluid theory, however, for the reflected type the Mach number will be unity at the throat. Fig. 23 presents the pressure ratio required across the nozzle diaphragm over a range of test section Mach numbers. Comparing this figure with Fig. 19 it is seen that there is a reduction in the pressure ratio required for starting in the reflected case.

6.4 THE TAILORED-INTERFACE MODIFICATION

The test time in the reflected shock type of tunnel is limited to the time interval between the arrival of the initial shock wave at the nozzle and the return of the secondary wave generated by the shock-contact surface interaction. A considerable increase in testing time is possible if the reflected shock can be made to pass through the contact front without producing any additional waves. This type of tunnel derives its name from this impedance matching or "tailoring", and two examples are illustrated in Fig. 24. If a second convergent-divergent nozzle is placed at the initial diaphragm station then the supersonic portion of the rarefaction wave can be eliminated and the reflected shock will traverse the full length of the driven section before returning to the downstream nozzle. In this case the driver section must be long enough to ensure that the reflected rarefaction wave does not reach the downstream nozzle before the reflected shock wave returns. One disadvantage of the method is that the area ratio of the nozzle at the initial diaphragm station must be changed for each Mach number.

If the reflected shock wave passes through the contact front without creating any additional waves the driver and driven gases must be at equal pressure and velocity behind the reflected shock. As the driver and the driven gases already are at equal pressure and velocity ahead of the reflected shock wave, the pressure ratio and velocity difference across the reflected shock are the same for the two gases. This may be stated mathematically with the aid of Fig. 24. The conditions for nonreflected waves are as follows. ⁽⁴⁰⁾

$$\frac{P_1}{P_2} = \frac{P_5}{P_3} = P \quad (6:4:1)$$

$$\frac{u_5 - u_2}{a_2} = \frac{u_1 - u_3}{a_3}$$

In the second of these two equations we have a Mach number and the speed of sound. In this case the strength of the incident and transmitted shocks are equal only if expressed in terms of their pressure ratios. The change in velocity across the shock may be expressed in the following manner.

$$\frac{\Delta u}{a} = \left[\frac{2}{\gamma(\gamma-1)} \right]^{\frac{1}{2}} \frac{P-1}{\left(1 + \frac{\gamma+1}{\gamma-1} P \right)^{\frac{1}{2}}} \quad (6:4:2)$$

Combining (6:4:1) and (6:4:2) gives

$$\frac{\gamma_2 (\gamma_2 - 1) \left(1 + \frac{\gamma_2 + 1}{\gamma_2 - 1} P \right)}{a_2^2} = \frac{\gamma_3 (\gamma_3 - 1) \left(1 + \frac{\gamma_3 + 1}{\gamma_3 - 1} P \right)}{a_3^2} \quad (6:4:3)$$

This equation must be satisfied whenever a shock passes through a contact surface without creating a reflected wave. For equal values of γ the equations then depend solely on the speeds of sound in states (2) and (3). This would be the case for a H_2 /Air combination. Therefore knowing the initial pressure p_1 , the shock wave Mach number and the driver gas then the required initial pressure and temperature of the driver gas can be calculated.

Figures 25 and 26 give the initial diaphragm pressure ratio and the initial driver gas temperature required for tailoring over a range of test Mach numbers for helium and hydrogen drivers. It is seen from Fig. 26 that helium at room temperature will tailor at a Mach number of 7.5, hydrogen at 10.6. In order to use the tailored interface technique at higher Mach numbers the driver gas must be heated. Figure 27 gives the variation of flight Mach number with shock Mach number for these conditions. Another disadvantage of the steady configuration, indicated by the figures, is the increased pressure and temperature of the driver gas required for this modification. However the steady tailored interface method produces test times three times greater than the unsteady modification and twenty-five times the nonreflected method. A comparison of testing times is shown in Fig. 28.

6.5 REAL GAS EFFECTS IN A HYPERSONIC SHOCK TUNNEL

In Section 5 the real gas effects in the production of strong shocks were considered. A brief consideration will be given here of the real gas effects on the design of a hypersonic shock tunnel, using an expansion nozzle. Figure 29 indicates the variation of test section

Mach numbers for a range of shock Mach numbers for a real gas, calculated for an equilibrium test section static temperature of 218°K, corresponding to the isothermal atmosphere. The curve for the ideal gas case is also shown for comparison, and is approximately 6 per cent lower than the real gas results. The density variation is shown in Fig. 30 and the real gas values are decreased compared to the ideal gas. Figure 31 presents the area ratio variation and, as would be expected from the density results, the real gas area ratio is considerably increased. In the reflected type the temperatures ahead of the nozzle may be high enough for dissociation to occur. When the gas is expanded through the nozzle the cooling rate will be very high and some of the constituents such as NO may be frozen. Another problem encountered using the reflected method is the loss of energy by radiation from the hot gas behind the reflected shock, which becomes more important as testing times are increased. These increased test times are possible using the tailored interface modification and so the radiation losses will have to be considered in a shock tunnel of this type.

6.6 REYNOLDS NUMBER AND STAGNATION TEMPERATURE SIMULATION

In order to do hypersonic testing it is desirable to simulate free flight conditions as closely as possible. This means simulating Mach number, stagnation temperature and Reynolds number. In the straight shock tube it is possible to simulate the temperature and Reynolds number but the Mach number is limited to a value of three as shown in Fig. 13. The use of expansion nozzles at the downstream end of the driven section.

enables the flow to expand to a high Mach number but in doing so may limit the other two conditions. The correct Reynolds number and stagnation temperature are controlled by the initial condition before the test gas enters the nozzle and thereby the strength of the initial shock wave. Figures 32 and 33 show the Reynolds number variation with test Mach number for a perfect gas, ($\gamma = 1.4$) and a test section static temperature of 518.4°R for a range of pressures behind the initial shock wave. Due to the decrease of density caused by the real gas effects (Fig. 30) the actual Reynolds number will be lower than those shown. For a given static pressure in the driven section, higher Reynolds numbers are realized with the nonreflected technique. Even though the Reynolds numbers shown here are lower than those possible in region (2) of a straight shock tube this may not be important as the Reynolds number of a body traveling at a hypersonic Mach number (≈ 20), at high altitude (100,000 ft.), is relatively low ($2 \times 10^6/\text{ft.}$). Therefore the attainment of a high Reynolds number will not be difficult for this class of problems.

7 CONCLUDING REMARKS

This report has attempted to outline the basic theory of the shock tube and describe most of the modifications to the basic tube that have been devised for hypersonic testing. Detailed calculation and theory have been omitted but these may be found in the many references cited.

REFERENCES

1. Bleakney, W.
Weimer, D. K.
Fletcher, C. H. The Shock Tube: Facility for Investigations in Fluid Dynamics, Ref. Sci. Inst. V. 20, No. 11, 1949
2. Glass, I. I.
Martin, W.
Patterson, G. N. A Theoretical and Experimental Study of the Shock Tube, UTIA Report No. 2, November 1953
3. Hertzberg, A. The Application of the Shock Tube to the Study of High Temperature Phenomena in Gases, Appl. Mech. Rev. 9, Dec. 1956
- 4a. Glass, I. I. Shock Tubes, Part I: Theory and Performance of Simple Shock Tubes, UTIA Review No. 12, Part I, May 1958
- 4b. Hall, J. G. Shock Tubes, Part II: Production of Strong Shock Waves, Shock Tube Applications, Design and Instrumentation, UTIA Review No. 12, Part II, May 1958
5. Hall, J. G. The Transition Through the Contact Region, UTIA Report No. 26, 1954
6. Wheeler, Donald B. Jr. Density Variation in Shock Tube Flow, Lehigh University Institute of Research, Technical Report No. 8, 1956
7. Rose, P. H. On the Effect of Attenuation of Gas Dynamic Measurements Made in Shock Tubes, AVCO Research Laboratory Research Report No. 24, April 1958
8. Resler, E. L., Lin, S. C.
Kantrowitz, A. The Production of High Temperature in Shock Tubes, J. Appl. Phys. Vol. 23, No. 12, 1952
9. Henshall, B. D. The Use of Multiple Diaphragms in Shock Tubes, Aero Res. Council London, Current Paper No. 291, December 1955
10. Alpher, R. A. Flow in Shock Tubes with Area Change at the Diaphragm Station, J. of Fluid Mechanics, Vol. 6, Part 3, Feb. 1958
11. Lukasiewicz, J. Shock Tube Theory and Application, National Aeronautical Establishment, Canada, Report No. 15, 1952
12. Hertzberg, A. The Shock Tunnel and its Applications to Hypersonic Flight, C.A.L. Rpt. No. AD-1052-A-5, June 1957

13. Henshall, B. D. The Theoretical Performance of Shock Tubes Designed to Produce High Shock Speeds, A.R.C. Report No. 20, 202, May 1958
14. Squire, W.
Hertzberg, A.
Smith, W. E. Real Gas Effects in a Hypersonic Shock Tunnel, C.A.L. Report No. AD-789-A-1 March 1955
15. Stollery, J. L. Real Gas Effects on Shock Tube Performance at High Shock Strengths, TN Aero 2143, November 1957
16. Logan, J. G. Jr.
Treasor, C. E. Tables of Thermodynamic Properties of Air from 3000°K to 10,000°K at Intervals of 100°K, C.A.L. Report No. BE-1007-A-3, January 1957
17. Gilmore, F. R. Equilibrium Composition and Thermodynamic Properties of Air to 24,000°K, Rand Corporation Research Memorandum, RM-1543, August 1955
18. Feldman, Saul Hypersonic Gas Dynamic Charts for Equilibrium Air, AVCO Research Laboratory, January 1957
19. Hilsenrath, Joseph
Beckett, Charles W. Tables of Thermodynamic Properties of Argon-Free Air to 15,000°K, National Bureau of Standards AEDC-TN-56-12, September 1956
20. Hochstim, A. R. Gas Properties Behind Shocks at Hypersonic Velocities I. Normal Shocks in Air, Convair, San Diego, Report No. ZPH (G.P.)-002, January 1957
21. Hochstim, A. R. Gas Properties Behind Shocks of Hypersonic Velocities II. Introduction to General Thermodynamics of a Real Gas, Convair, San Diego, Report No. ZPH-003, May 1957
22. Hochstim, A. R.
Areve, R. J. Gas Properties Behind Shocks at Hypersonic Velocities III. Various Thermodynamic Properties of Air, Convair, San Diego, Report No. ZPH-004, June 1957

23. Hochstim, A. R.
Gas Properties Behind Shocks at Hyper-sonic Velocities IV. Isentropic Charts for Air from 2000°K to 15,000°K, Convair San Diego, Report No. ZPH-005
24. Seigel, A. E.
Theoretical Study of the Effect of the Non-ideality of a Dense Shock-Tube Driver Gas with Special Reference to Non-uniform Shock Tubes, Proceedings of the Fourth U. S. Navy Symposium on Aeroballistics, Vol. 1, May 1958
25. Trimpi, R. L.
Cohen, N. B.
A Theory for Predicting the Flow of Real Gases in Shock Tubes with Experimental Verification, NACA TN-3375, 1955
26. Mirels, H.
Attenuation in a Shock Tube Due to Unsteady Boundary Layer Action, NACA TN-3278, August 1956
27. Mirels, H.
Braun, W. H.
Nonuniform in Shock-Tube Flow Due to Unsteady Boundary Layer Action, NACA TN-4021, April 1957
28. Jones, Jim J.
Experimental investigation of Attenuation of Strong Shock Waves in a Shock Tube with Hydrogen and Helium as Driver Gases, NACA TN-4072, July 1957
29. Mirels, H.
Boundary Layer Behind a Shock Advancing into a Stationary Fluid, NACA TN-3712, May 1956
30. Bershader, D.
Allport, J.
On the Laminar Boundary Layer Induced by a Travelling Shock Wave, Princeton Univ. TR II-22, May 1956
31. Martin, W. A.
An Experimental Study of the Boundary Layer Behind a Moving Plane Shock Wave, UTIA Report No. 47, May 1957
32. Gooderum, P. B.
An Experimental Study of the Turbulent Boundary Layer on a Shock-Tube Wall, NACA TN-4243, June 1958
33. Boyer, D. W.
Effects of Kinematic Viscosity and Wave Speed on Shock Wave Attenuation, UTIA TN No. 8, 1956

34. Hertzberg, A. A Shock Tube Method of Generating Hypersonic Flows, J. Aero. Sci. 18 (1951) Page 803
35. Parks, E. K. Supersonic Flow in a Shock Tube of Divergent Cross-Section, UTIA Report No. 18, May 1952
36. Henshall, B. D.
Gadd, B. A. Factors Affecting the Performance of the Nozzle of a Hypersonic Shock Tube, ARC Tech. Report 293, February 1956
37. Hertzberg, A.
Smith, W. E.
Glick, H. S.
Squire, W. Modifications of the Shock Tube for the Generation at Hypersonic Flow, Cal. Report No. AD-789-A-2, March 1955
38. Glick, H. S.
Hertzberg, A.
Smith, W. E. Flow Phenomena in Starting a Hypersonic Shock Tunnel, Cal. Report No. AD-789-A-3, March 1955
39. Wittliff, C. E.
Wilson, A. R.
Hertzberg, A. The Tailored-Interface Hypersonic Shock Tunnel. Paper Presented at the ASME-ARS Aviation Conference, Dallas, Texas, March 1958
40. Rudinger, G. Wave Diagrams for Nonsteady Flow in Ducts, D. Van Nostrand Co., Inc., New York, 1955

APPENDIX A

NOTATION

Figure 1 serves to define the flow regions in the basic shock tube. The notation Air/Air, He/Air and H₂/Air denotes a gas combination across the diaphragm, the left-hand symbol representing the gas in the driver section, the right-hand symbol the gas in the driven section.

a	Velocity of sound
A	Area
A_{1j}	Dimensionless speed of sound ratio (i.e. $A_{14} = a_1/a_4$)
C_{1j}	Dimensionless rarefaction wave speed
D	Diameter
E_{1j}	Dimensionless energy ratio $(C_v T)_i / (C_v T)_j$
g	Equivalence factor (Eq. 4.3.2)
L	Length
M_s	Shock Wave Mach number based on speed of sound of gas into which it travels
M	Mach number
p	Pressure
P_0	Overall pressure ratio (see Section 4.2)
P_{1j}	Dimensionless pressure ratio (i.e. P_2/P_1)
P_{4d}	Pressure in region (4), Fig. 4 for double diaphragm shock tube (Sect. 4.2)
P_{4s}	Pressure in region (4) for single diaphragm shock tube (Sect. 4.2)
t	Time
T	Temperature

T_{1j}	Dimensionless temperature ratio (i.e. T_2/T_1)
T_{1d}	Temperature in region (4), Fig. 4 for double diaphragm shock tube (Sect. 4.2)
T_{1s}	Temperature in region (4), for single diaphragm shock tube (Sect. 4.2)
u	Particle velocity
U_{1j}	Dimensionless particle velocity (i.e. u_2/a_1)
x	Position along the shock tube measured from the diaphragm
γ	Ratio of specific heats (c_p/c_v)
α	$\frac{\gamma+1}{\gamma-1}$
β	$\frac{\gamma-1}{2\gamma}$
ρ_{1j}	Dimensionless density ratio (i.e. ρ_2/ρ_1)
ν	Kinematic viscosity
ρ	Density
\vec{c}	Contact surface moving to the right
\vec{R}	Backward facing rarefaction wave (particles enter from left)
\vec{S}	Forward facing shock wave (particles enter from right)

Quantities not included here are defined in the text or on the figures in which they appear.

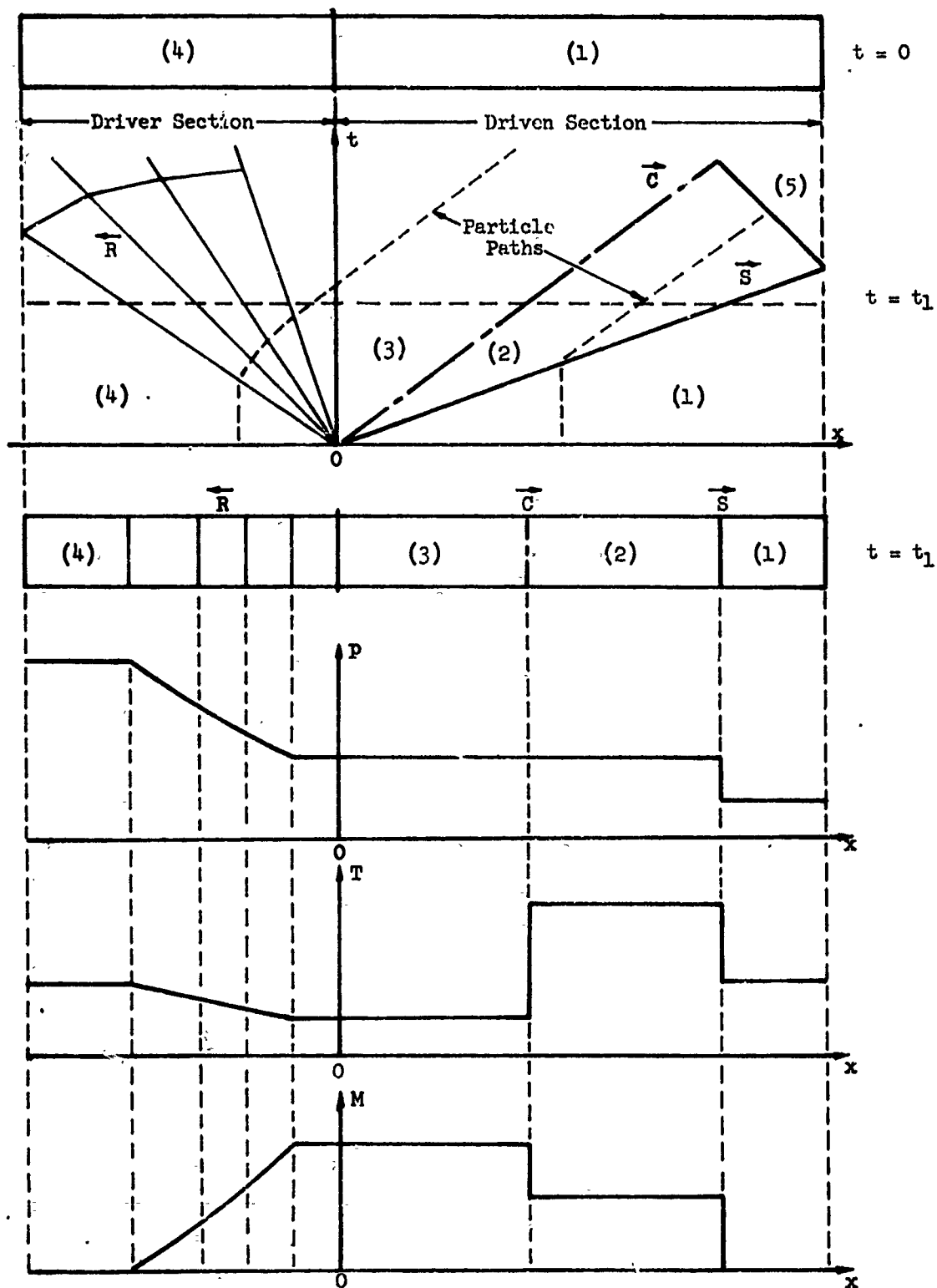


FIG. 1 - The Wave System in the Shock Tube. The Bottom Half of the Sketch Indicates the Pressure, Temperature and Mach No. at time, $t = t_1$.

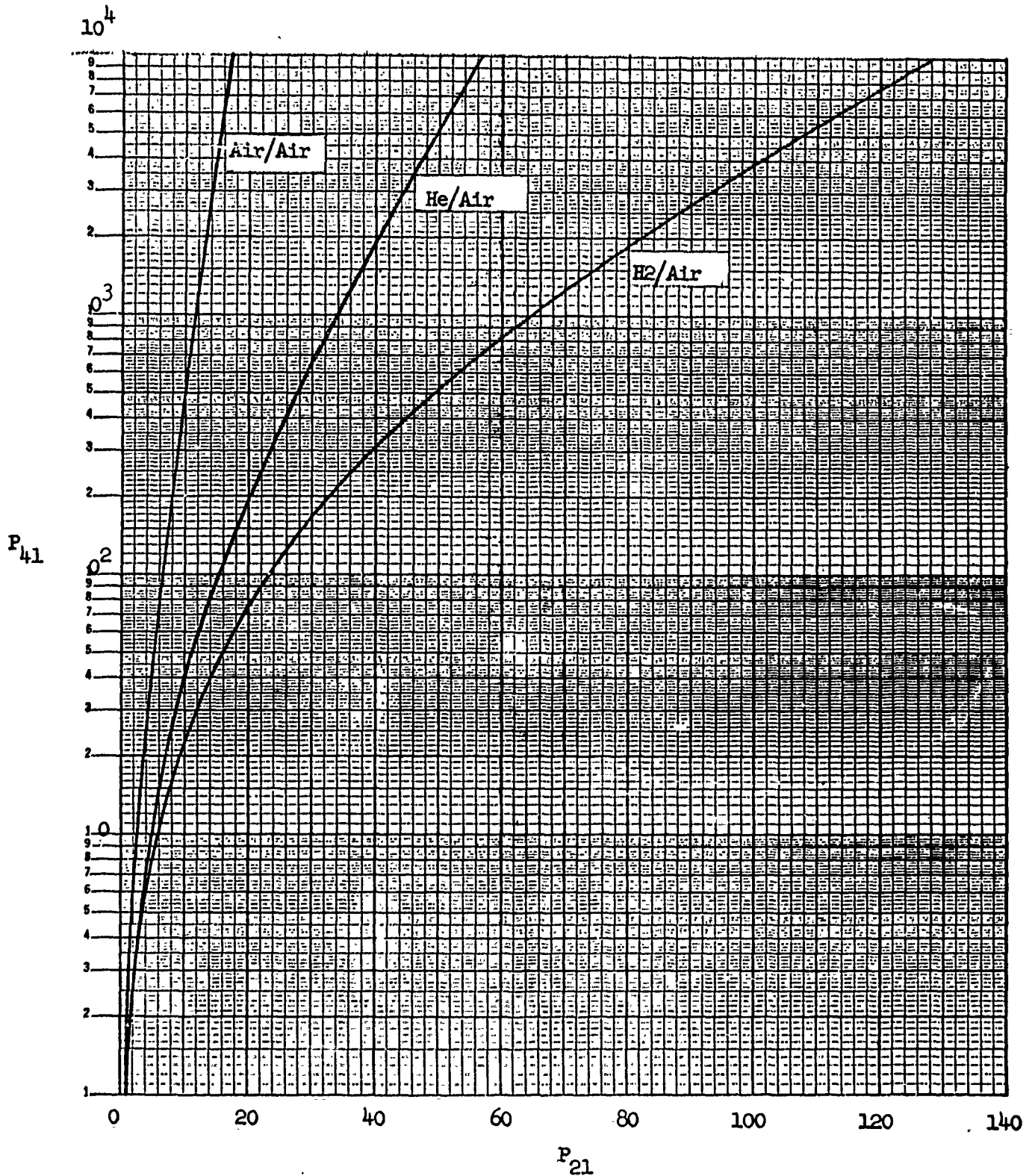


Figure 2 - Variation of Shock Pressure Ratio, P_{21} with Diaphragm Pressure Ratio, P_{41} , $\gamma = 1.4$.

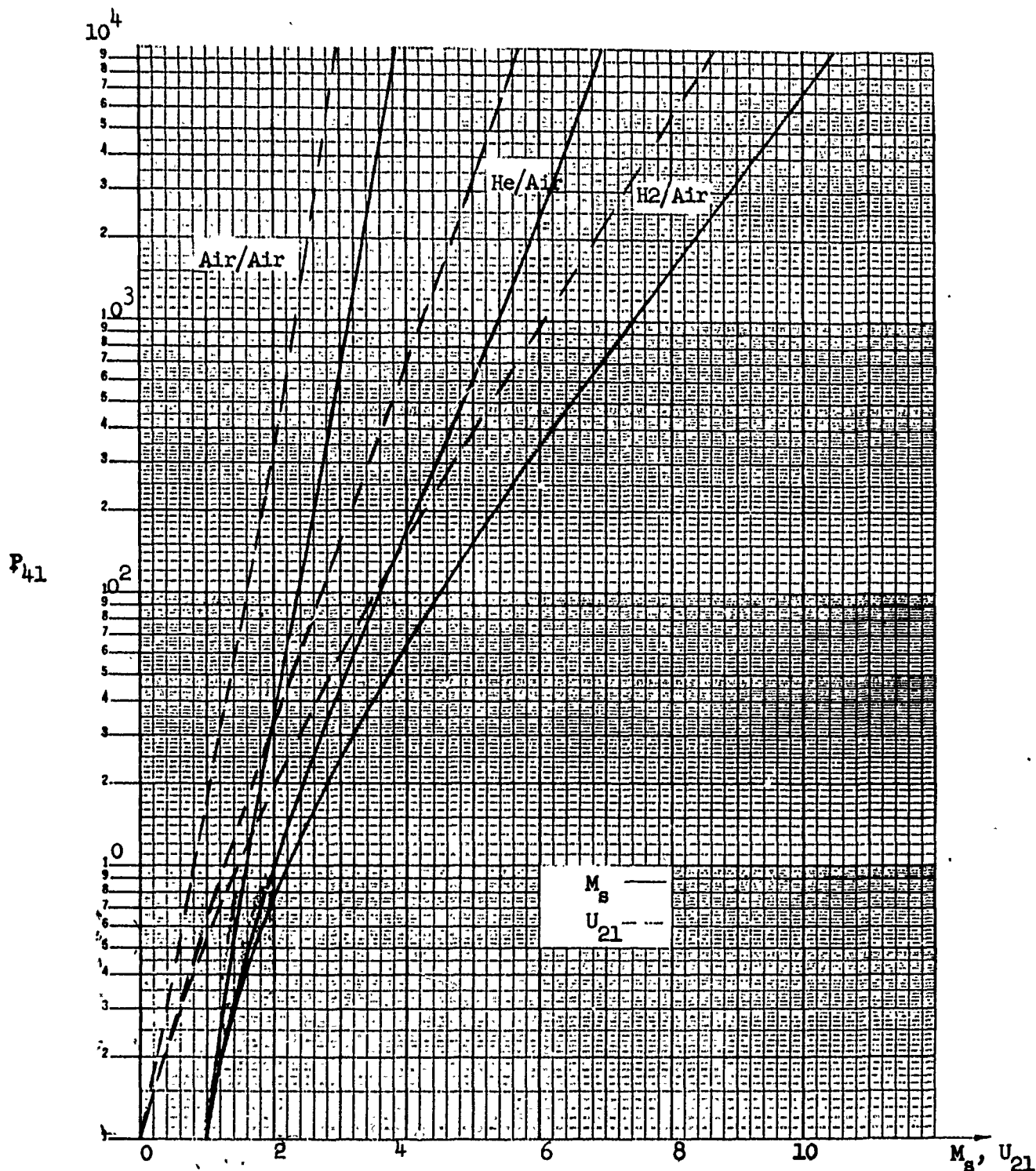


Figure 3 - Variation of Shock Mach Number, M_s and Particle Velocity, U_{21} , with Diaphragm Pressure Ratio, P_{41} for $\gamma_1 = 1.4$.

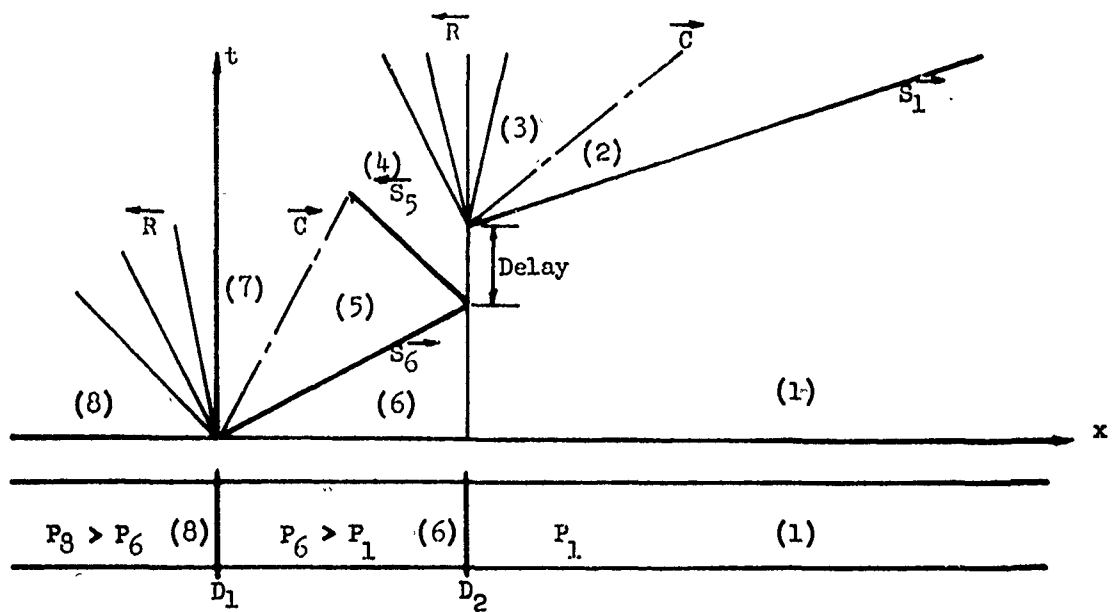


FIG. 4 - The Double Diaphragm Shock Tube - Reflected Shock Type

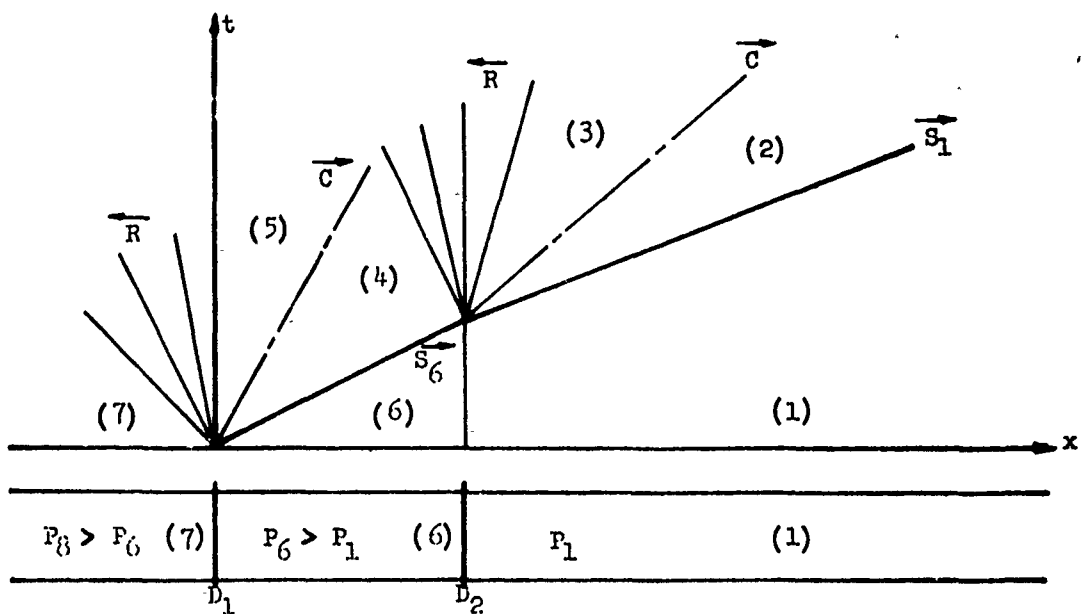


FIG. 5 - The Double Diaphragm Shock Tube - Unsteady Expansion Type

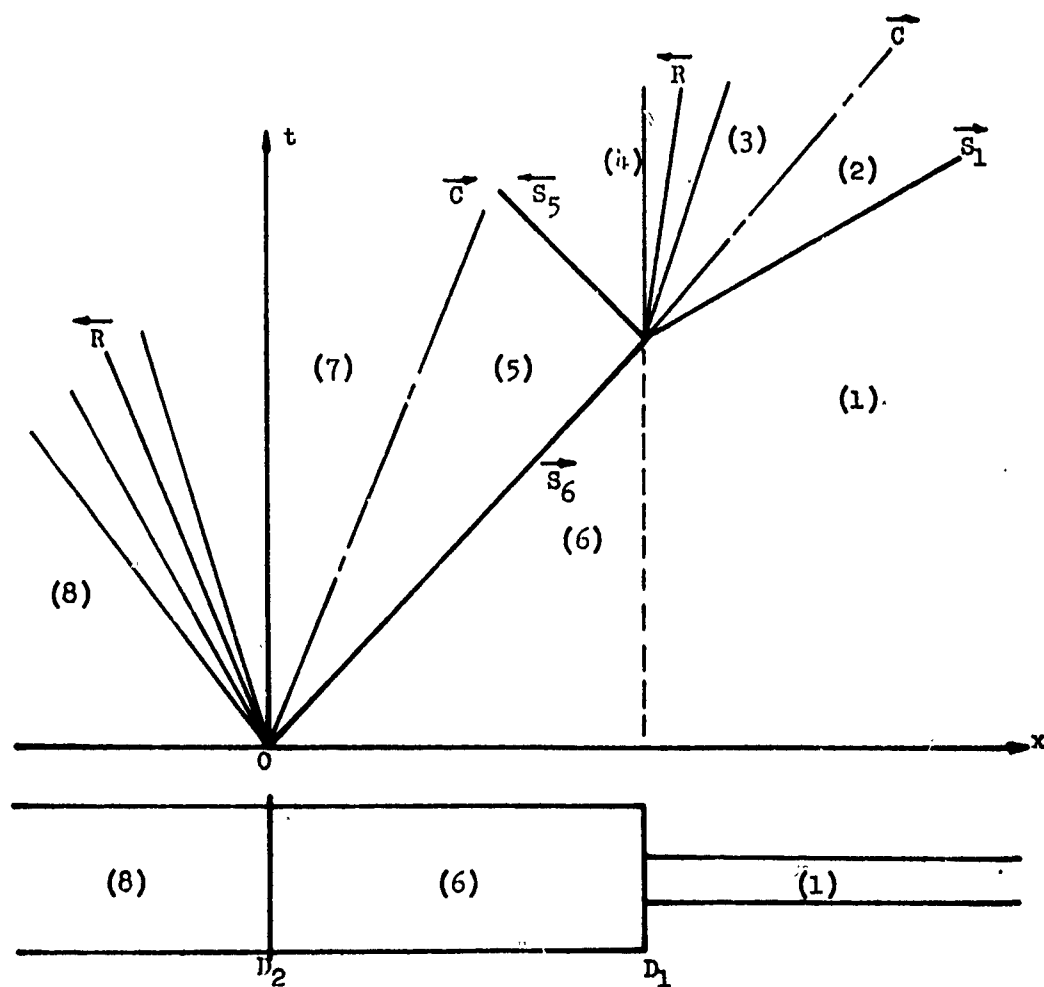


FIG. 6 - Shock Tube with an Area Discontinuity

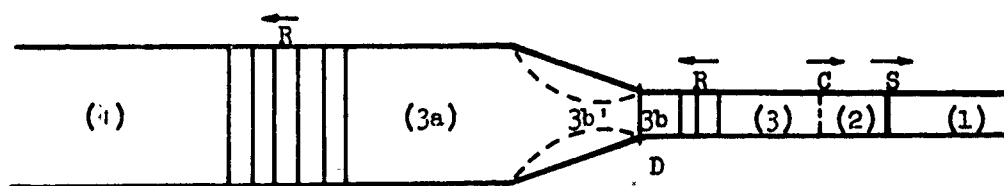


FIG. 7 - Shock Tube with a Convergent Transition Section. The dashed lines in the diaphragm section denote a convergent-divergent geometry with minimum area at 3b'

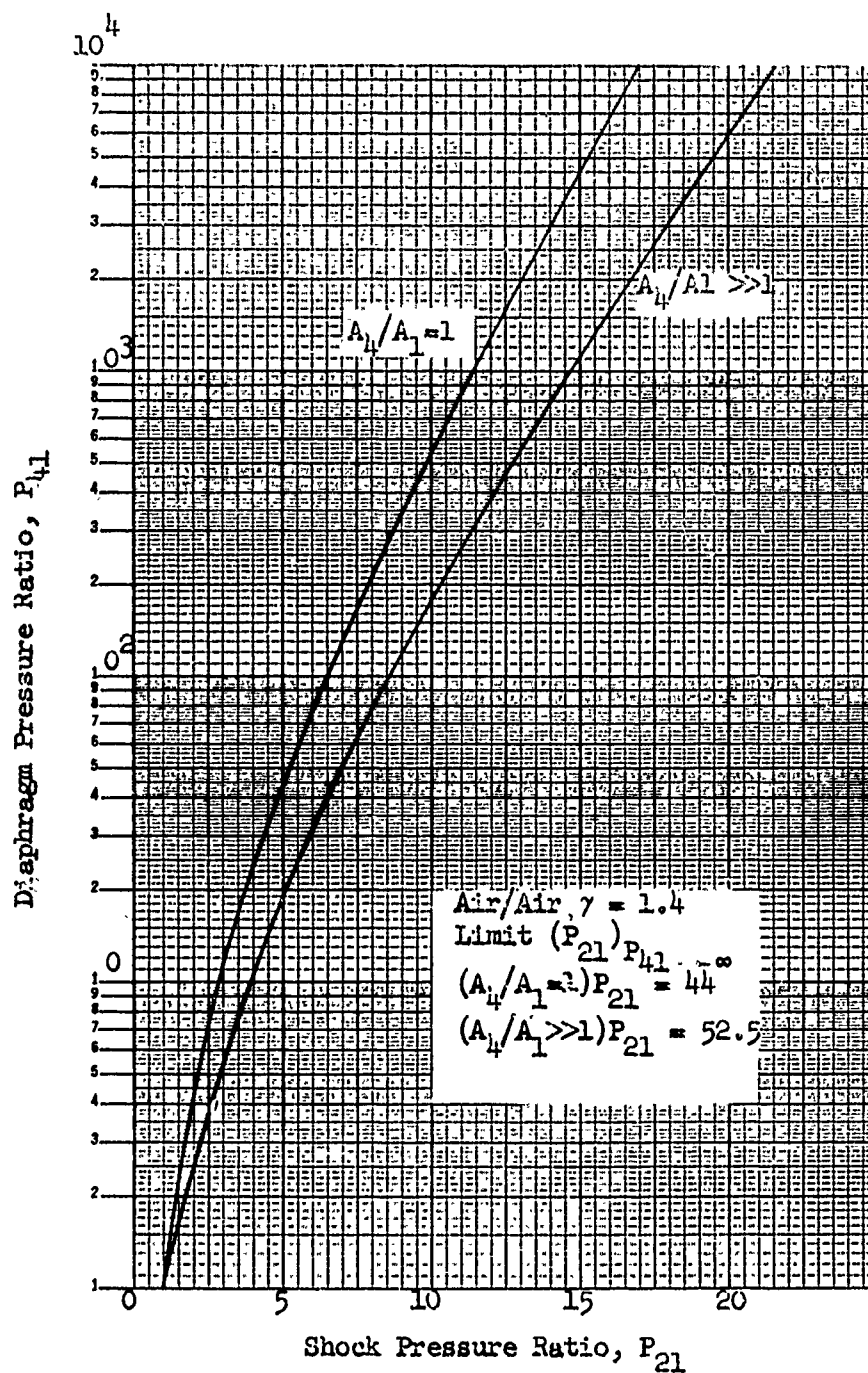


Figure 8 - Performance Comparison of a Variable Geometry and Simple Shock Tube, $\gamma = 1.4$.

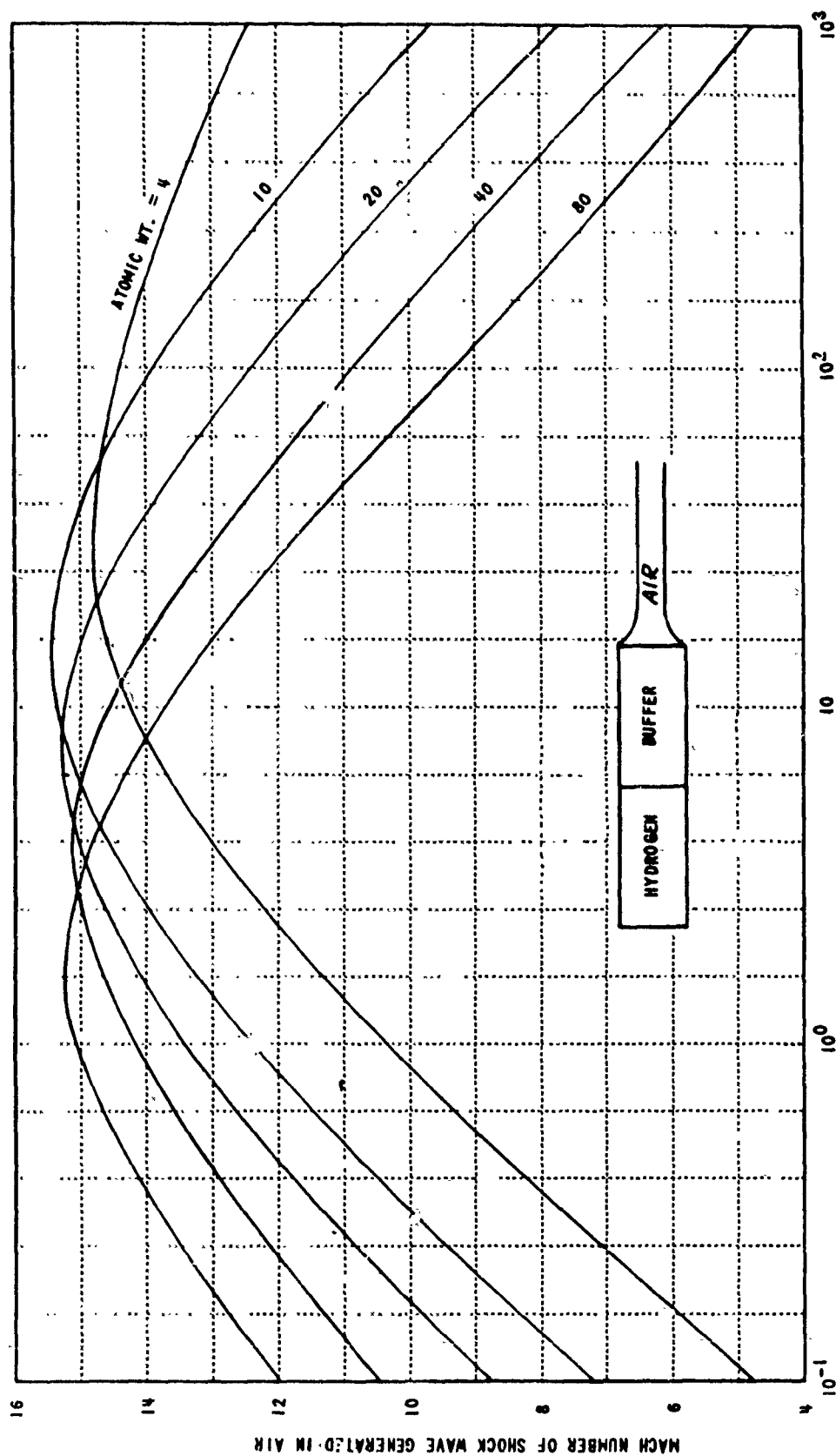


Figure 9 - Performance of a hydrogen-air shock tube with an over-all pressure ratio of 10,000 showing the effects of varying the pressure and molecular weight of the buffer gas (Ref. 12)

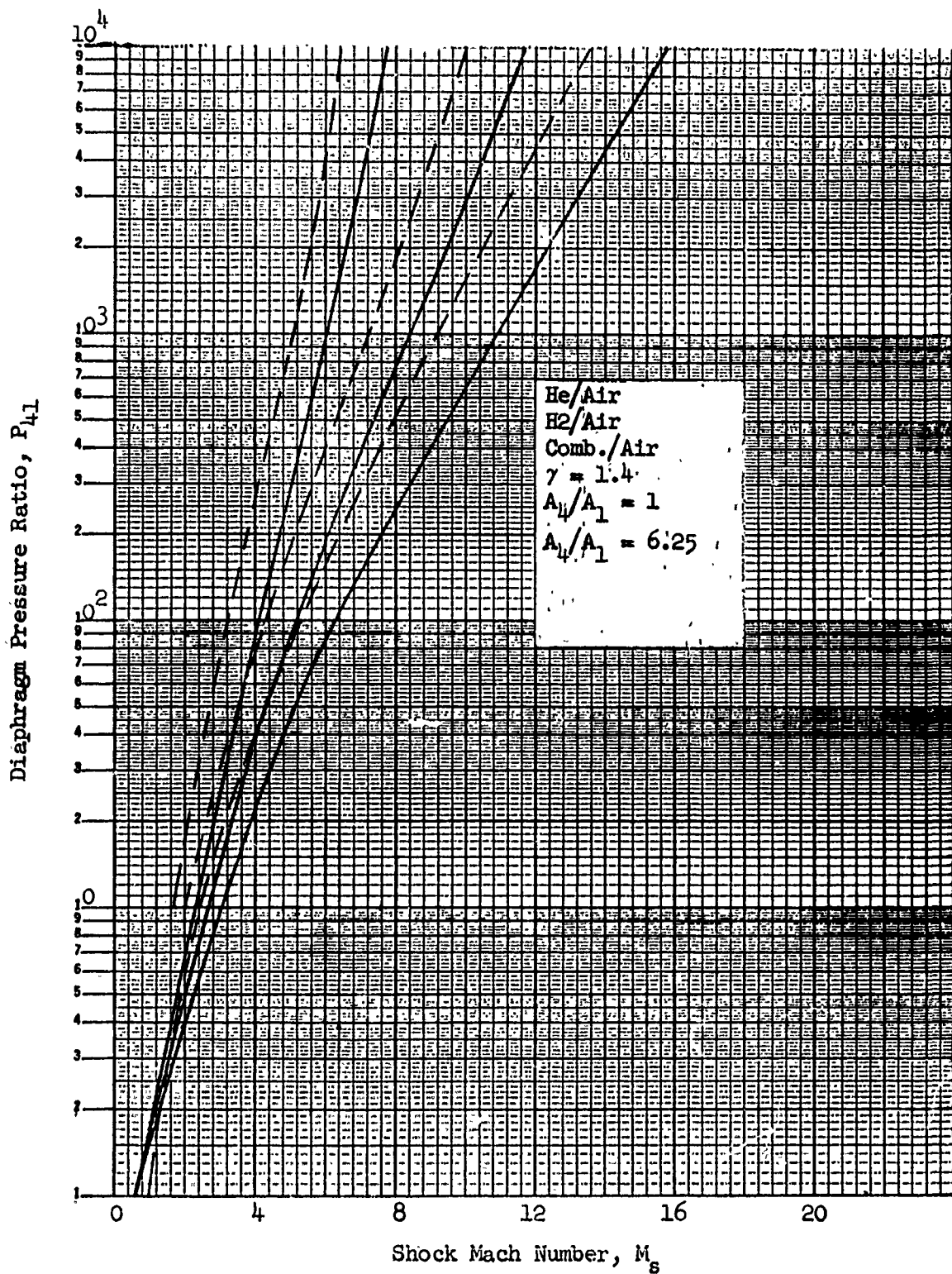


Figure 10 - Performance Comparison of Various Driver Gases for
 $A_4/A_1 = 1$ and $A_4/A_1 = 6.25$.

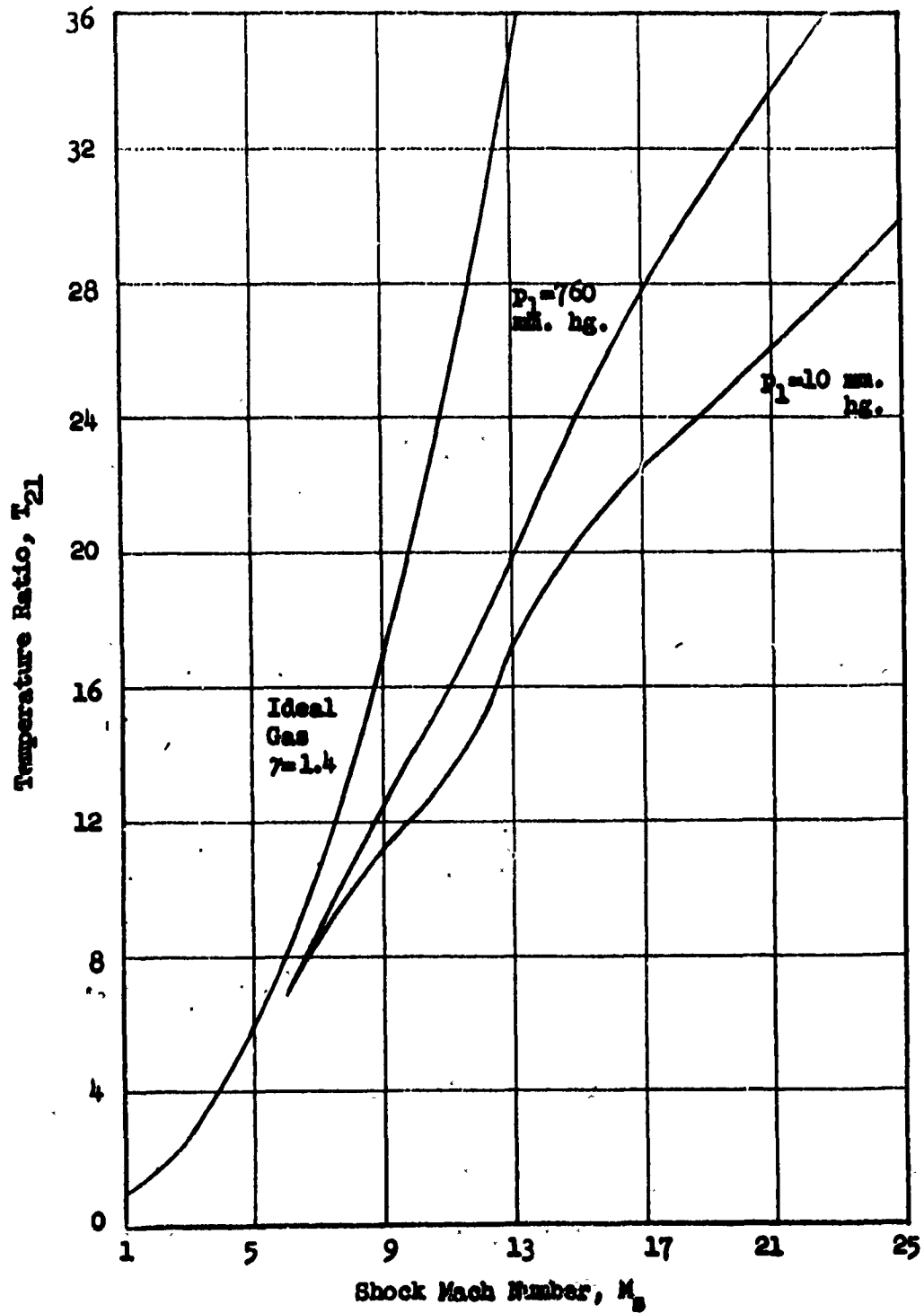


Figure 11 - Variation of Temperature Ratio, T_{21} with Shock Mach Number, M_s

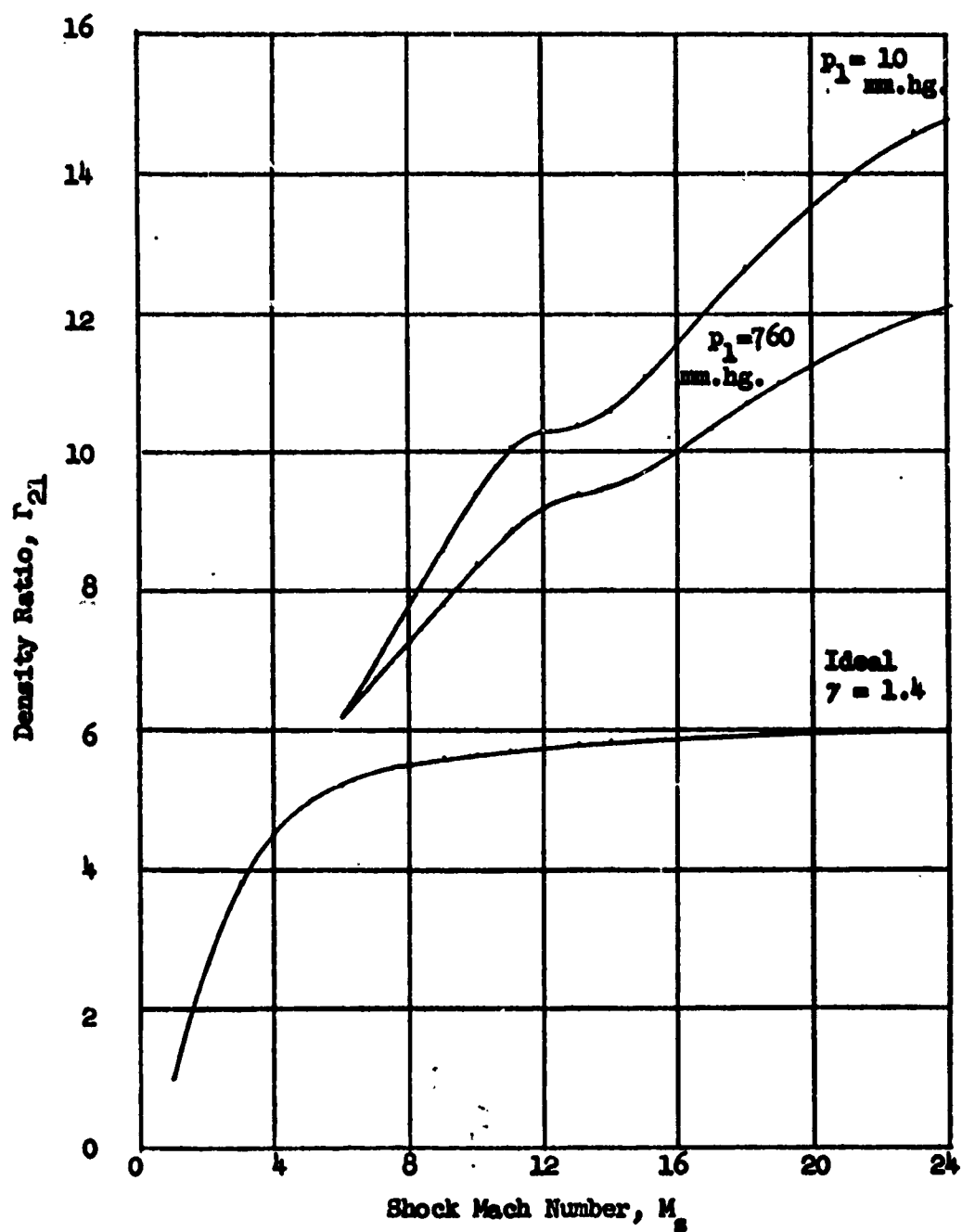


Figure 12 - Density Ratio Variation across the Initial Shock Wave.

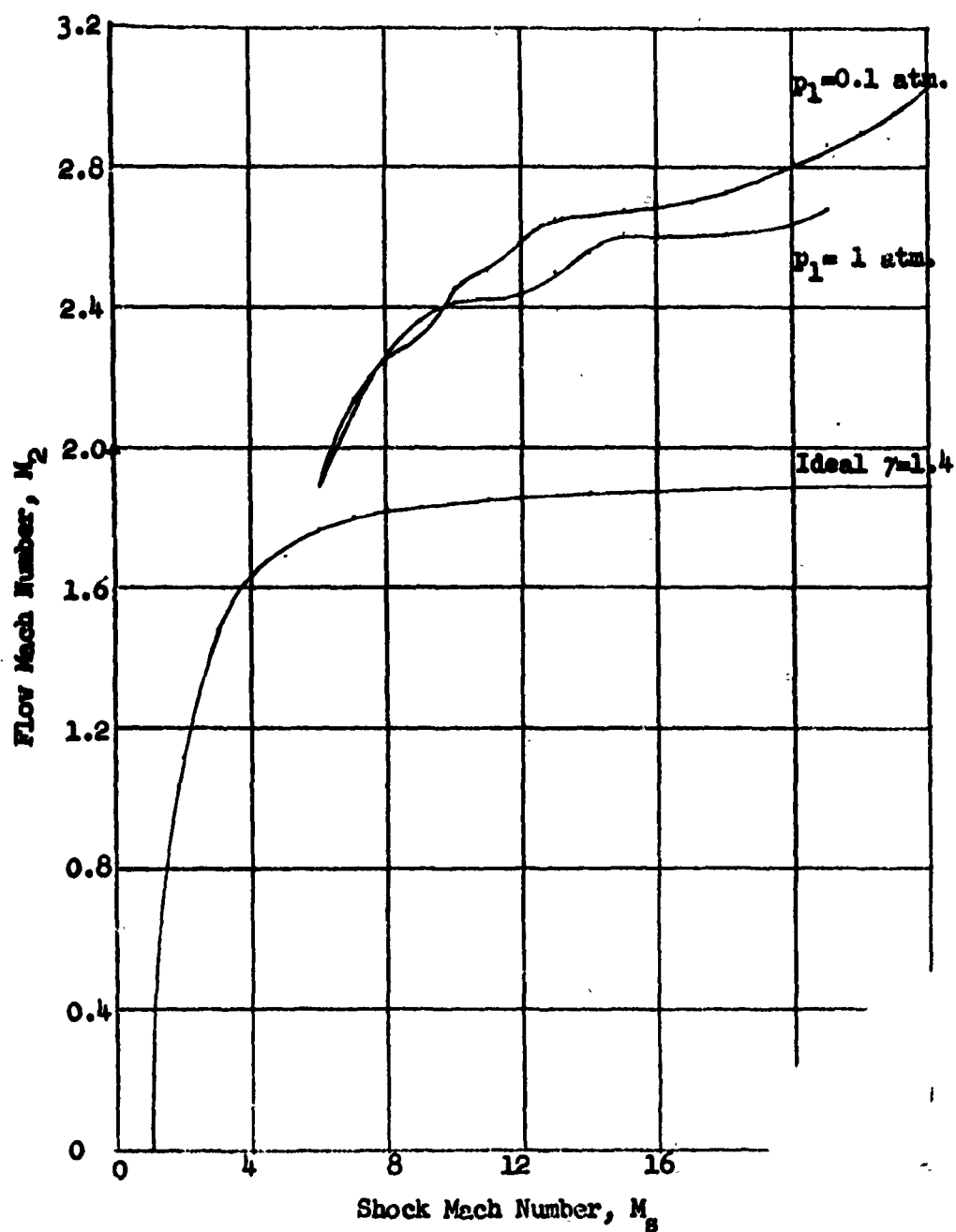


Figure 13 - Variation of Flow Mach Number behind Initial Shock Wave

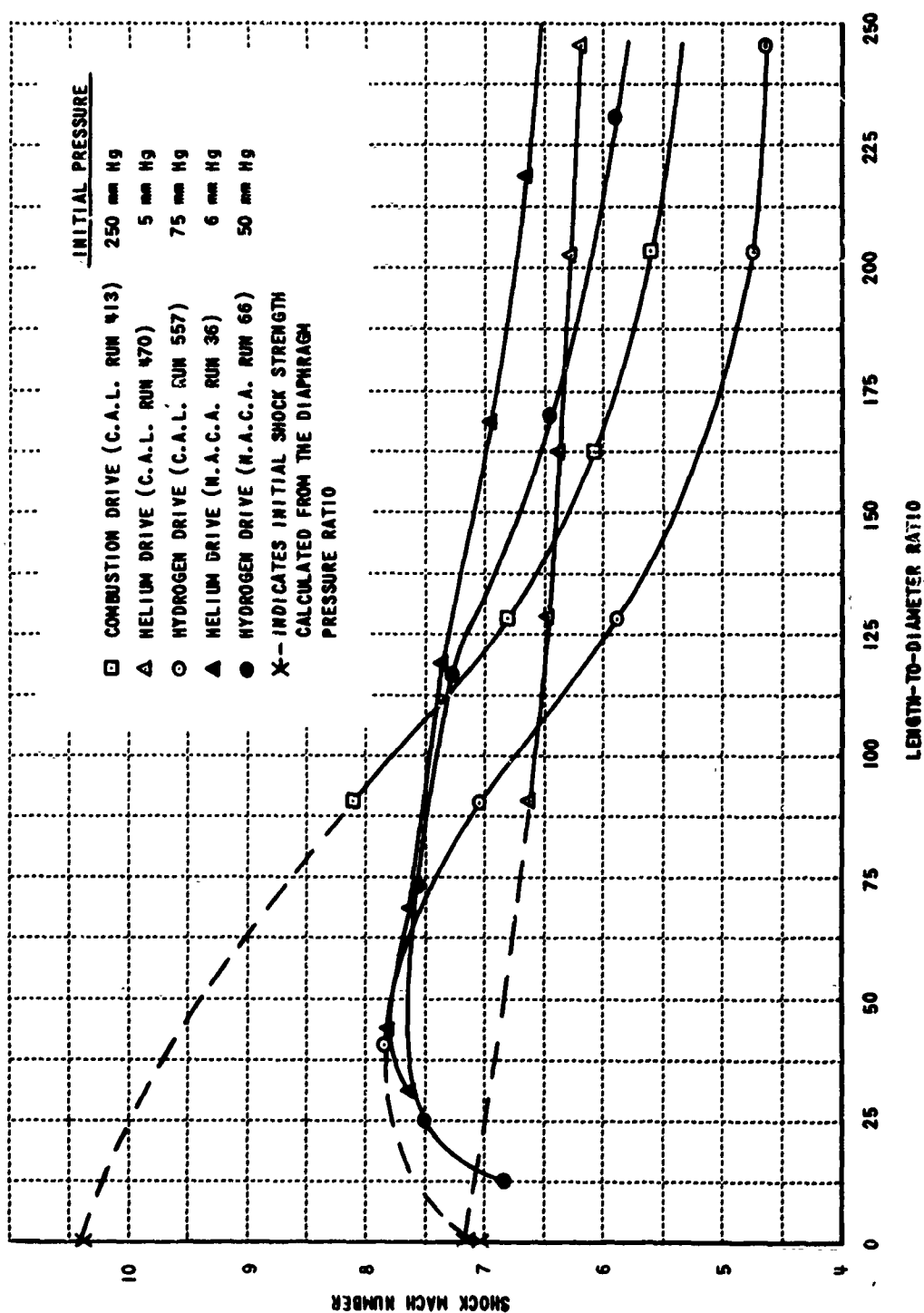


Figure 14 - Attenuation of strong shock waves in slender shock tubes (Ref. 12)

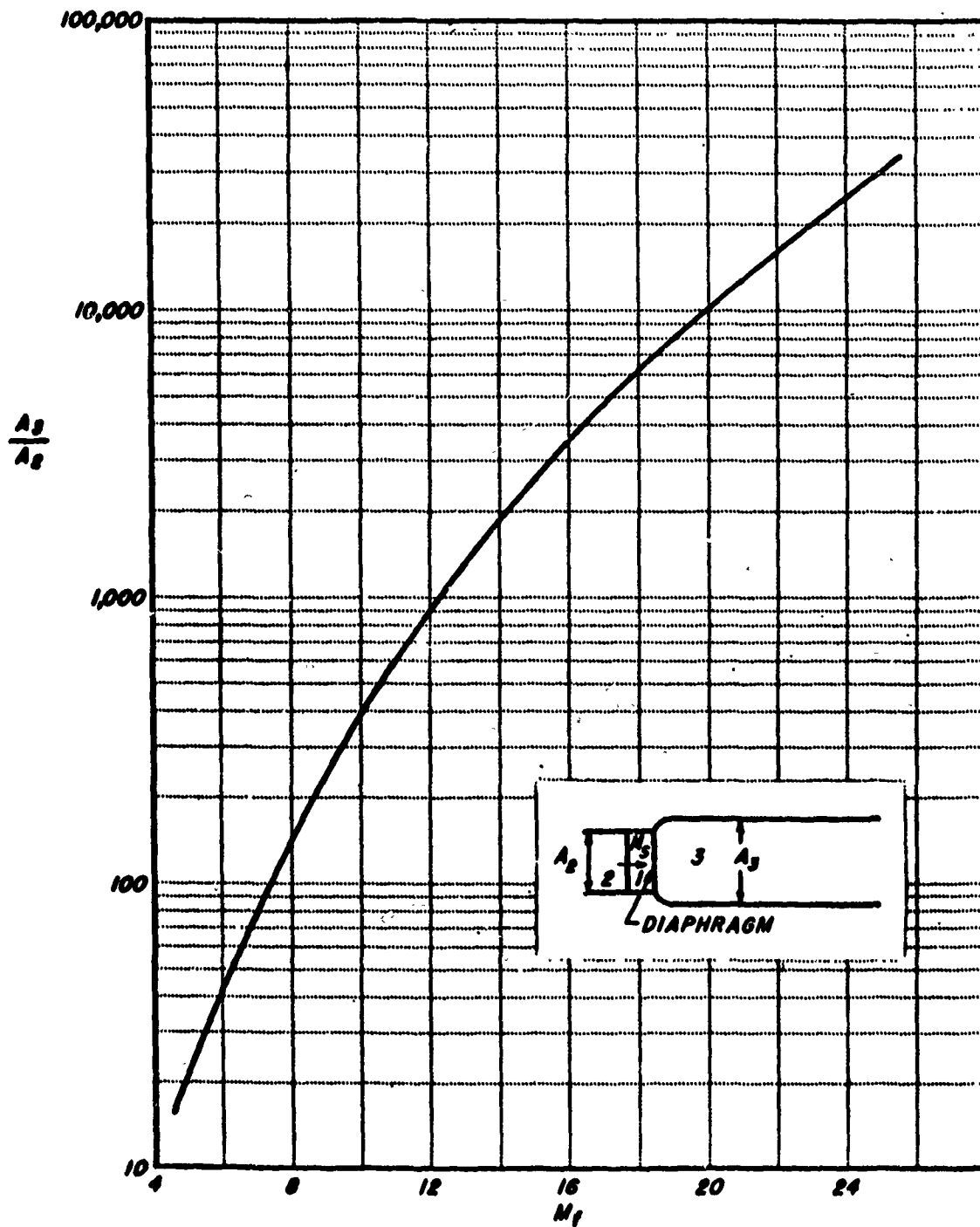


Figure 15 - Overall area ratio vs. flight Mach number ($\gamma = 1.4$, no reflection) (Ref. 38)

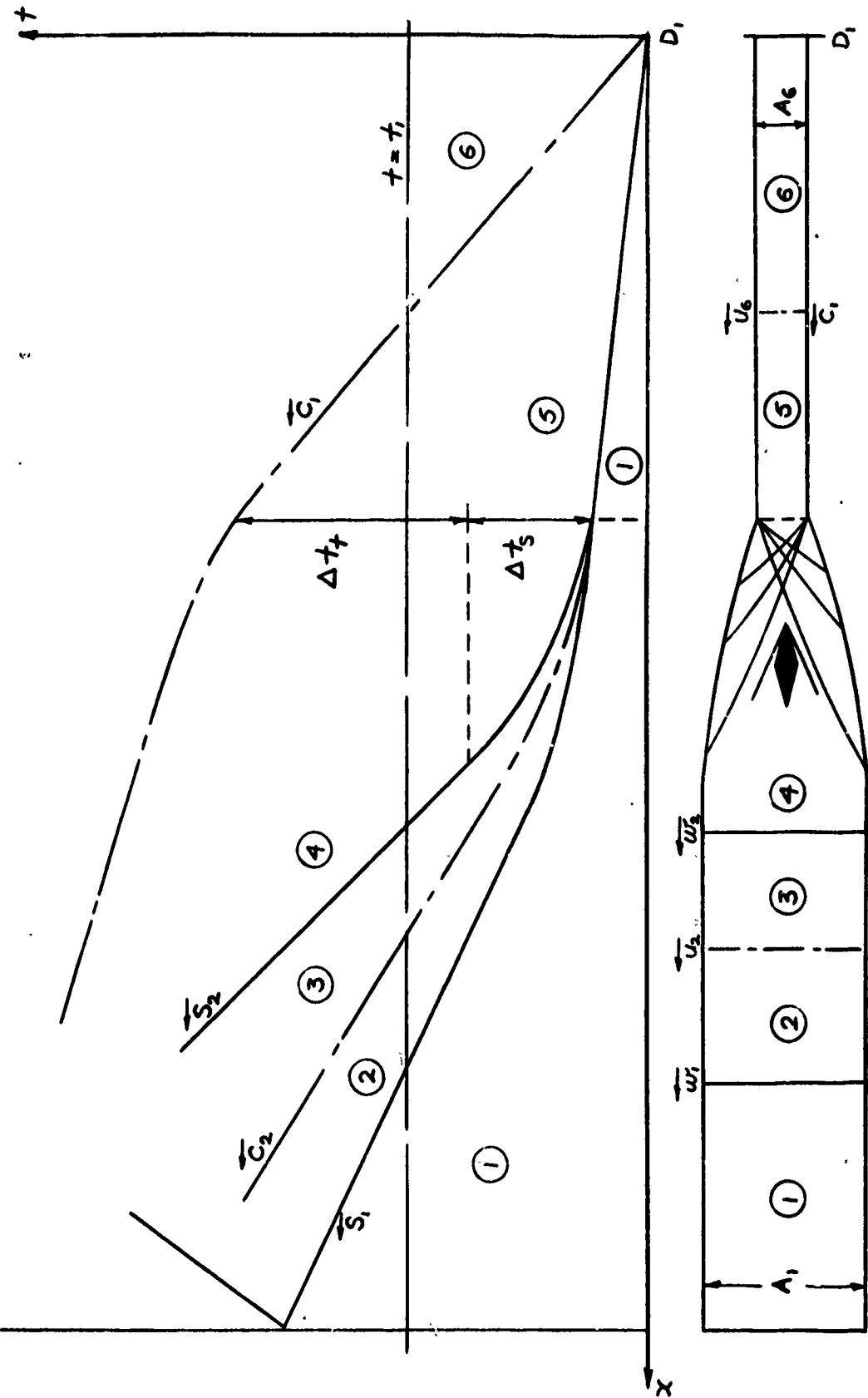


Figure 16 - Wave Diagram for a hypersonic shock tunnel.

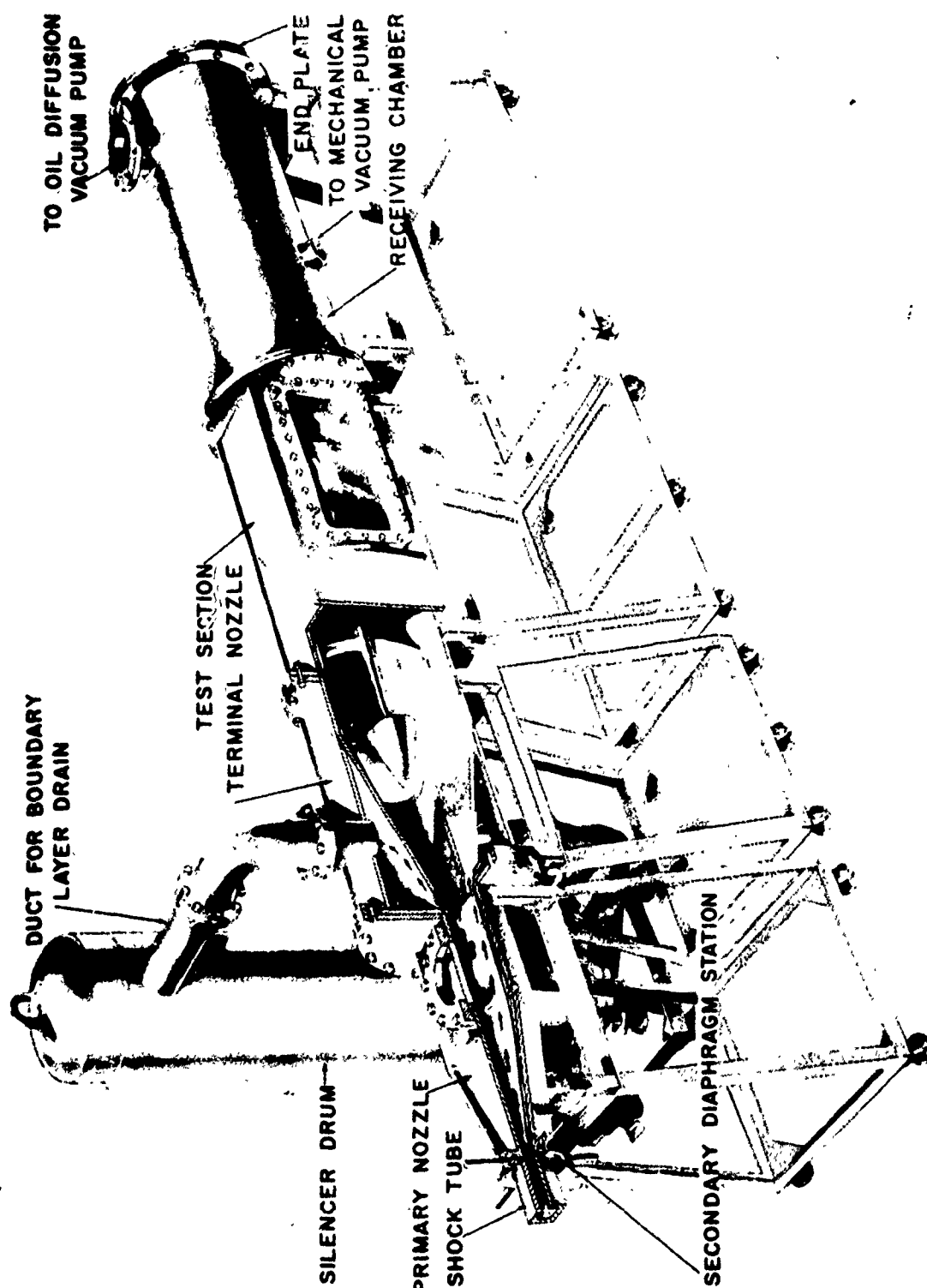


Fig. 17 - The Cornell Aeronautical Laboratory 11- By 15- Inch Hypersonic Shock Tunnel
(Ref. 12)

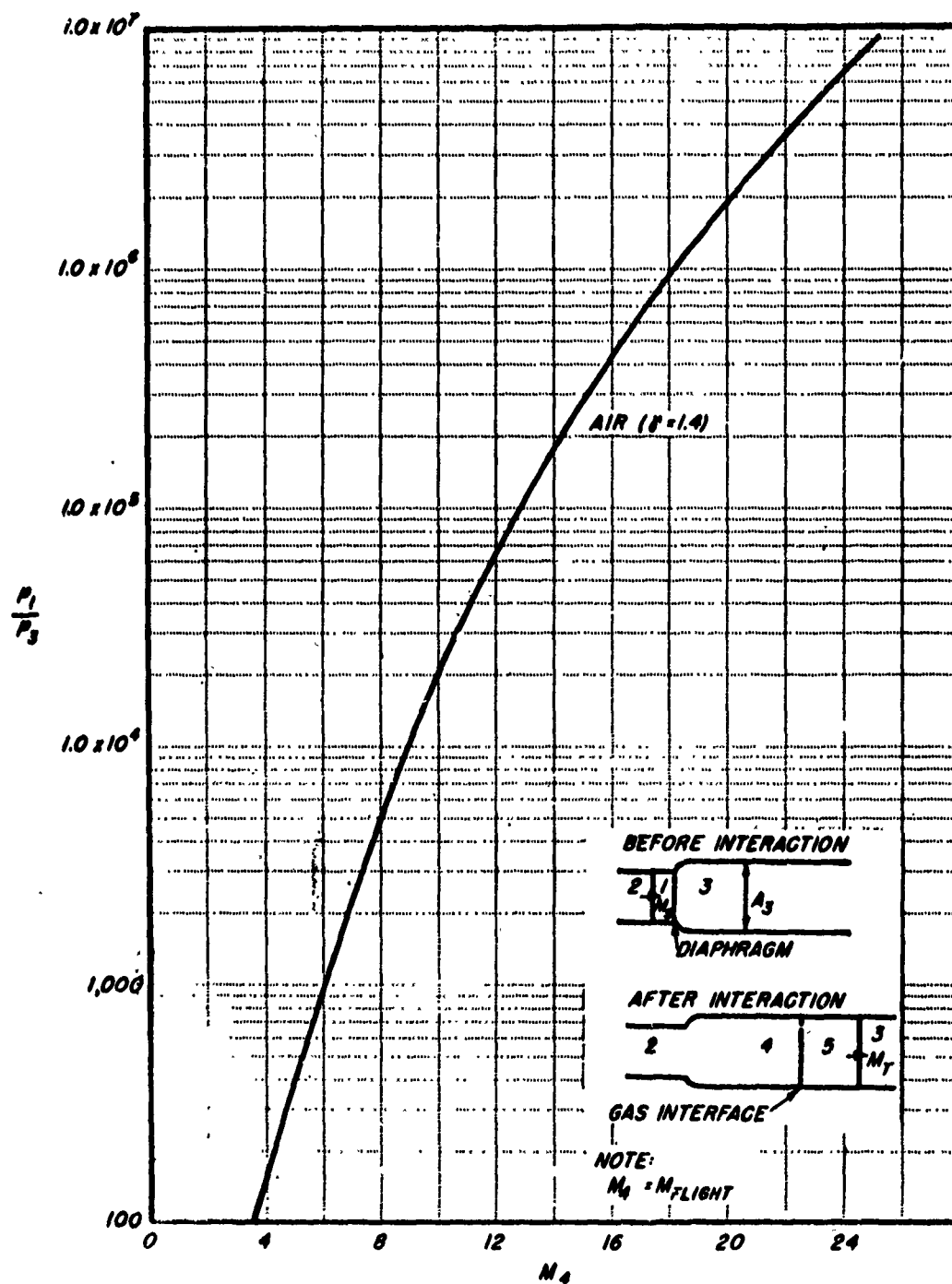


Figure 18 - Pressure ratio across diaphragm vs. flight Mach number for perfect starting (no reflection) (Ref. 38)

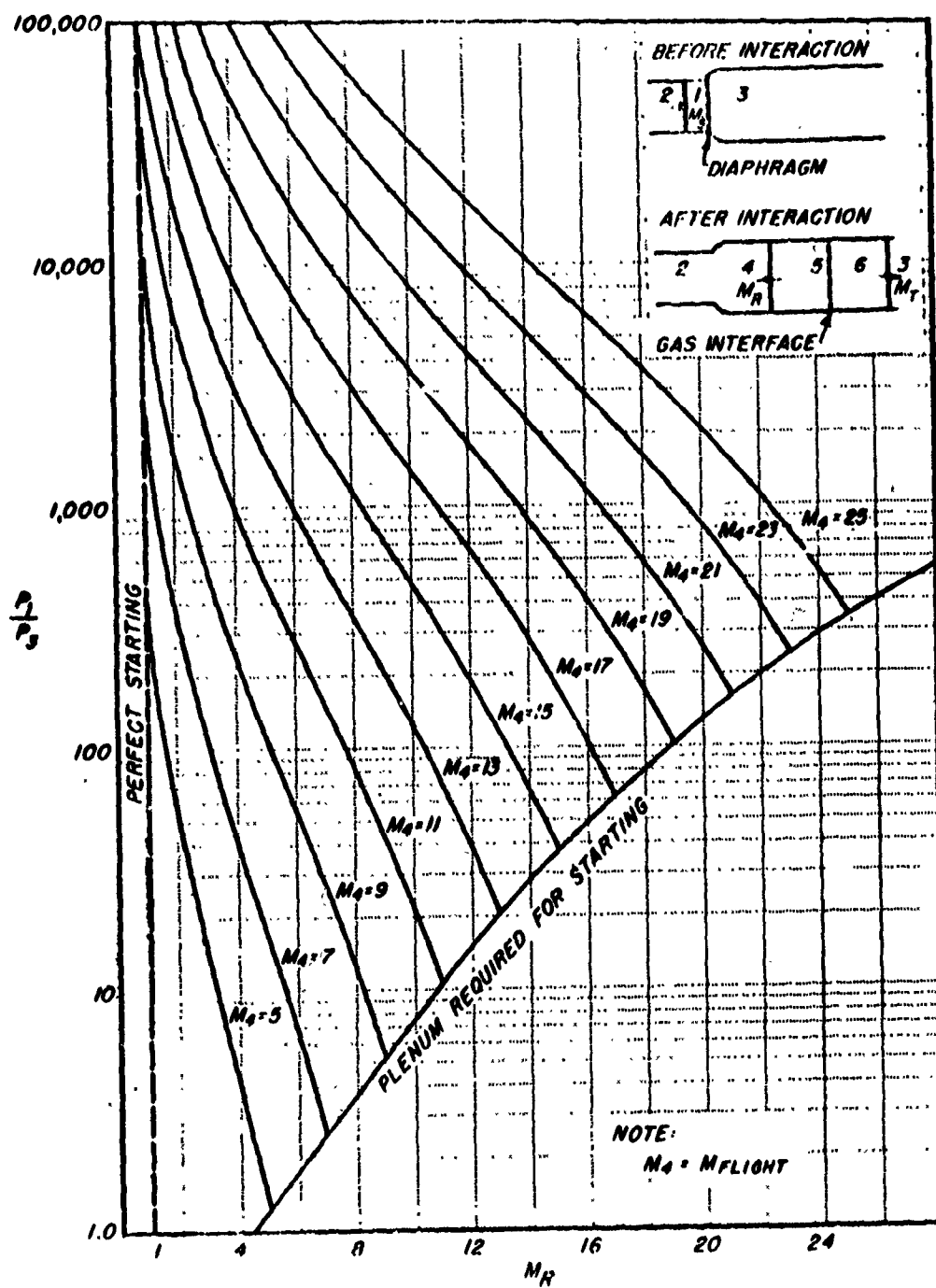


Figure 19 - Pressure ratio across diaphragm vs. strength of reflected shock ($\gamma = 1.4$, no reflection) (Ref. 38)

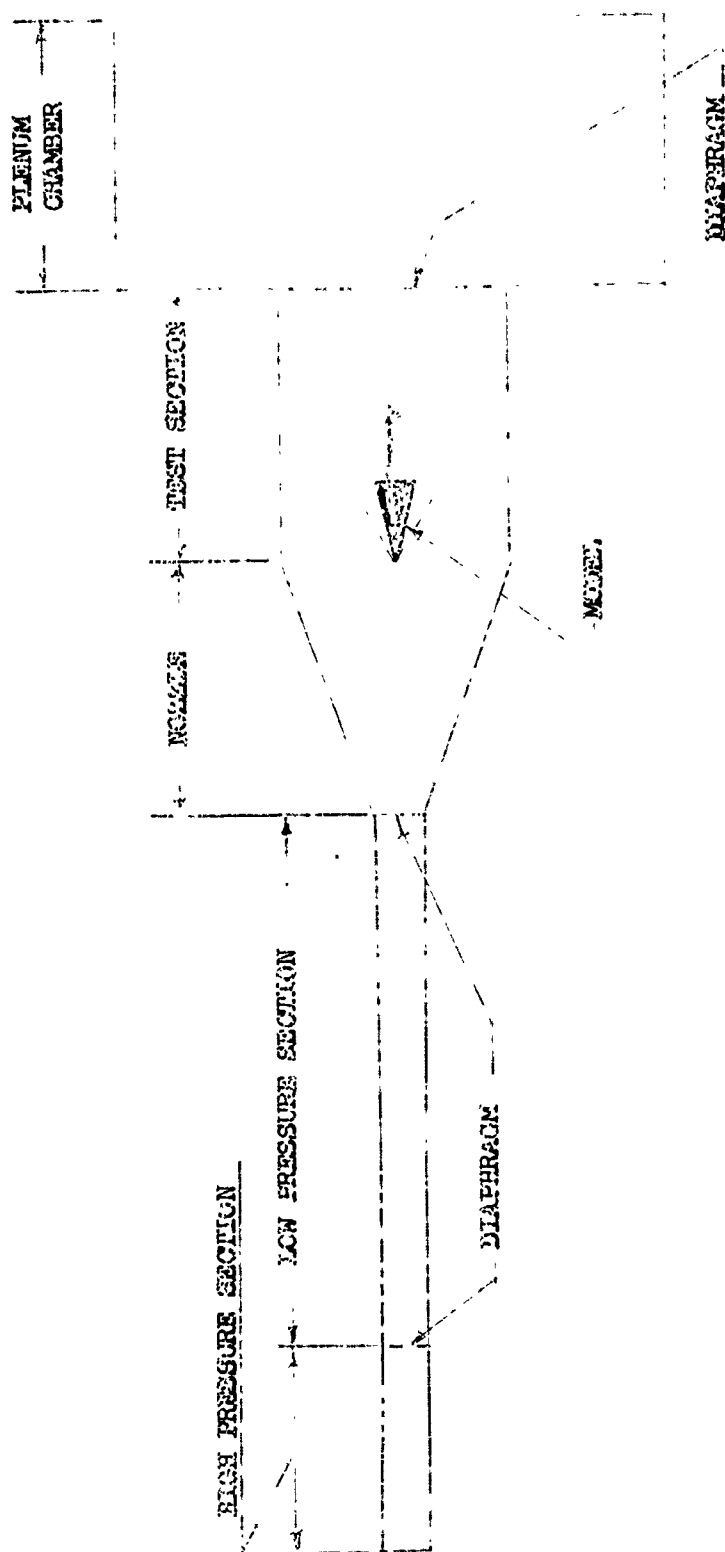


Figure 20 - Schematic drawing of hypersonic shock tunnel with plenum chamber.

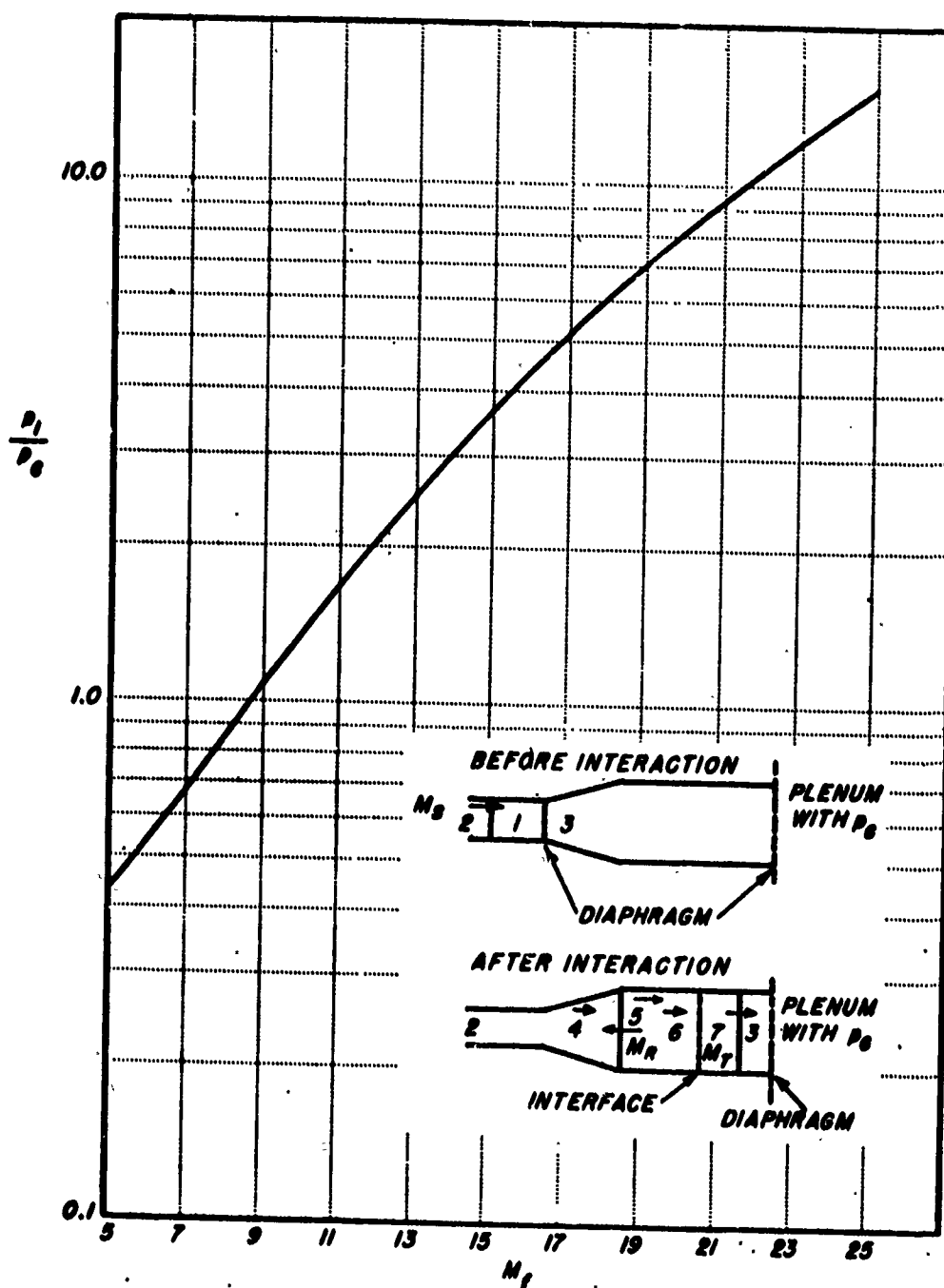


Figure 21 - Ratio of pressure in low pressure section to plenum pressure vs. flight Mach number for ideal gas ($\gamma = 1.4$, no reflection) (Ref. 38)

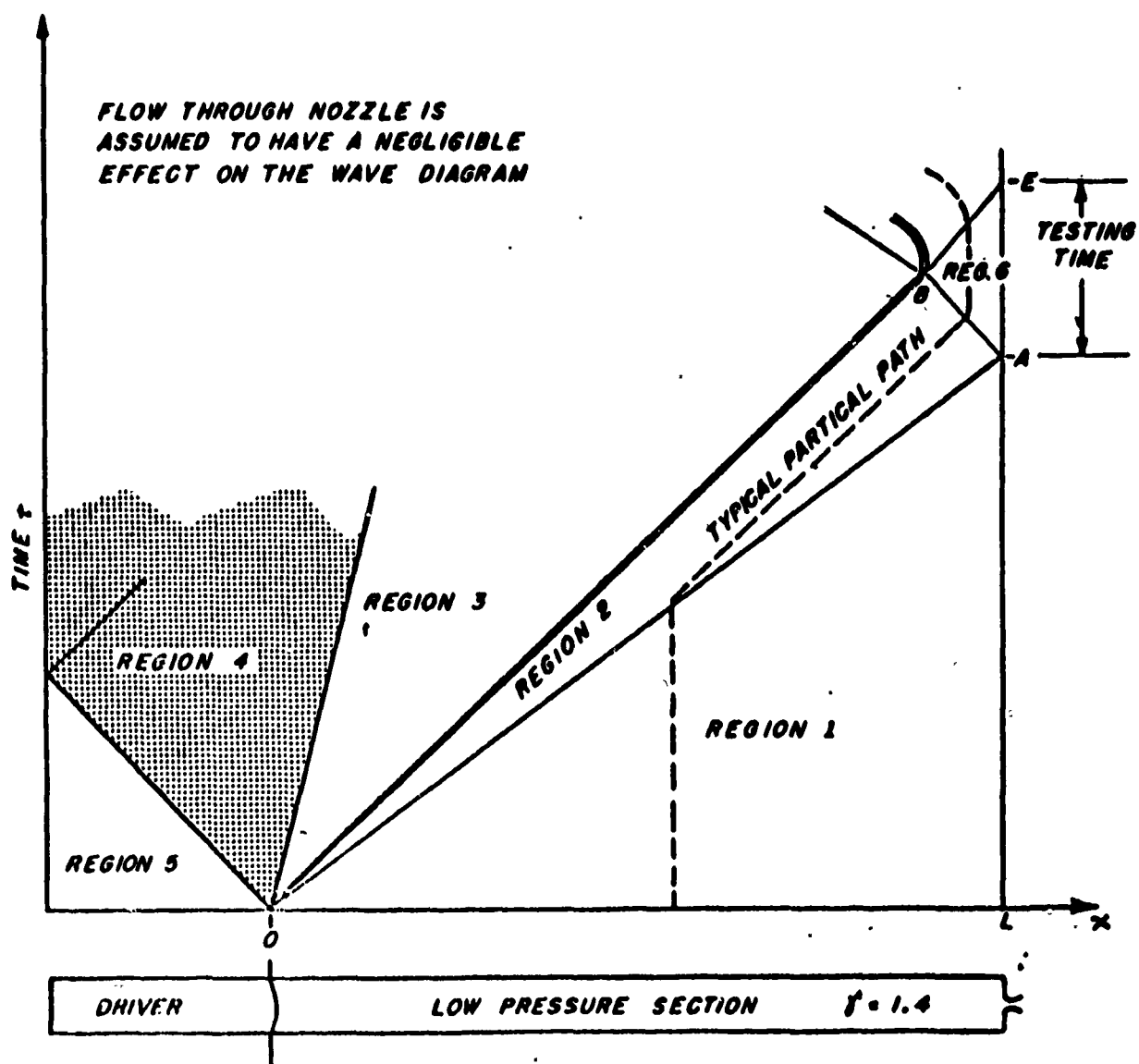


Figure 22 - Wave diagram for the reflected method. (Ref. 37)

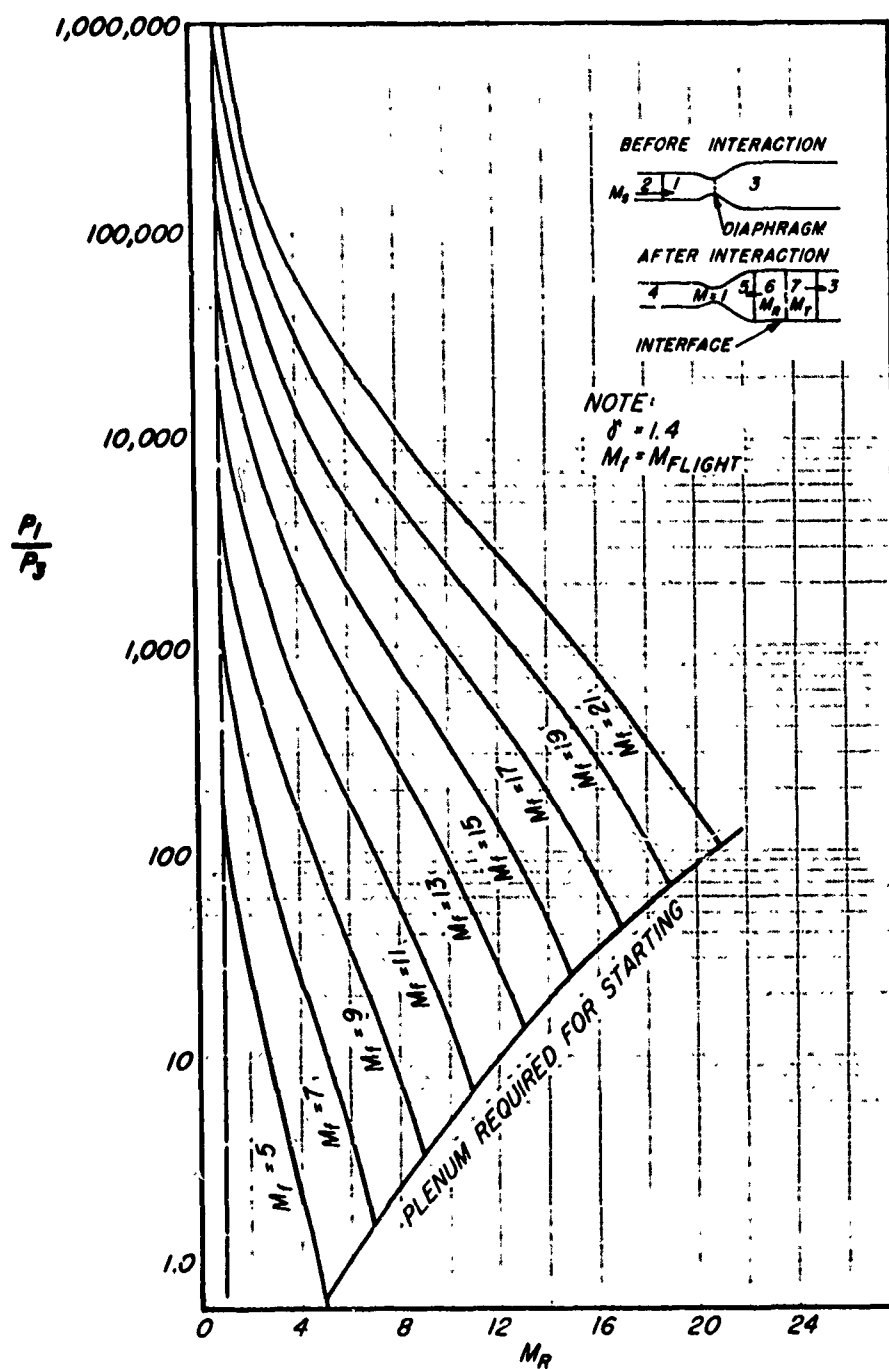


Figure 23 - Pressure ratio across diaphragm vs. strength of reflected shock. (Ref. 38)

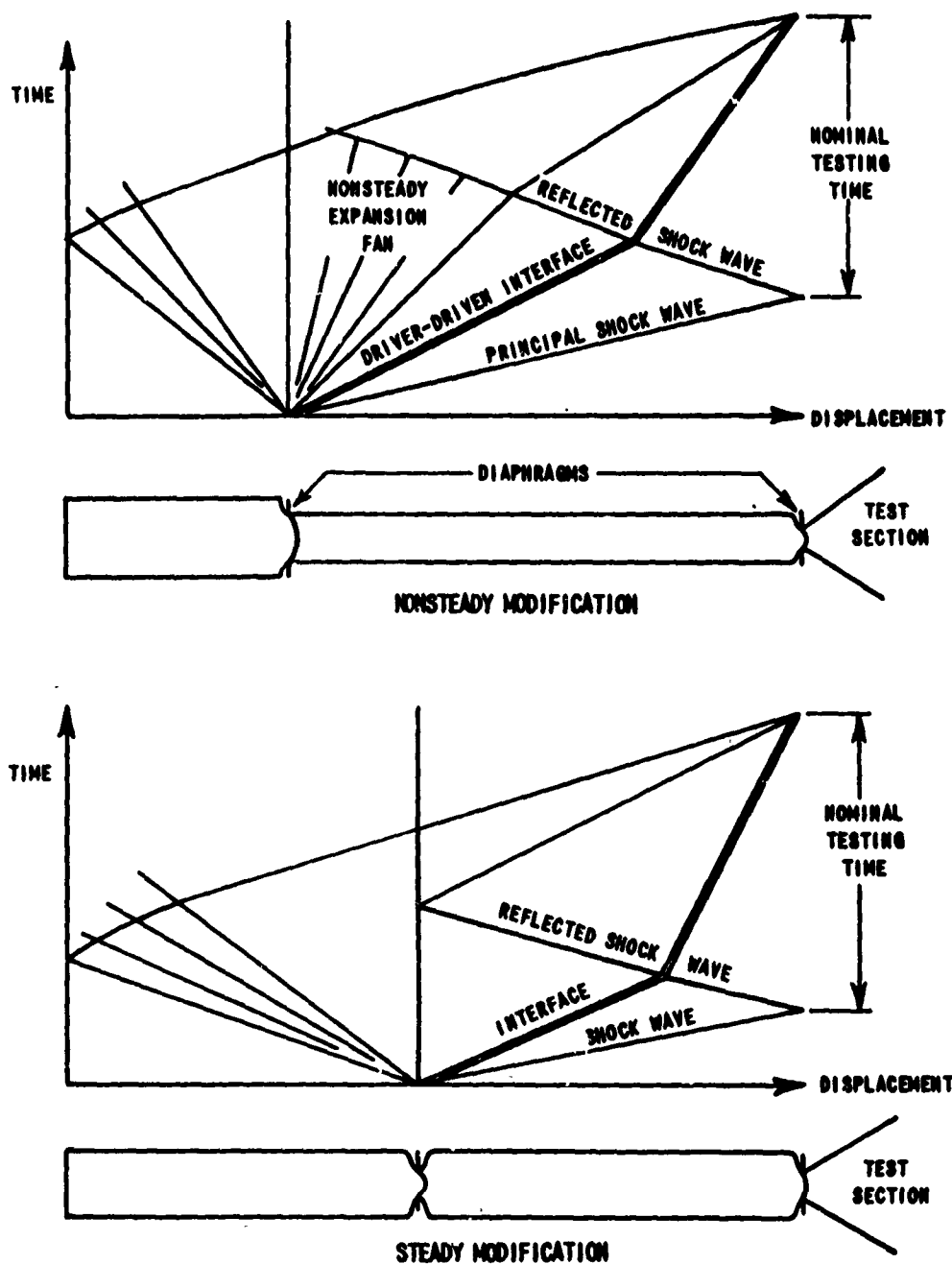


Figure 24 - Wave diagrams of shock tube modifications for increased testing time. (Ref. 12)

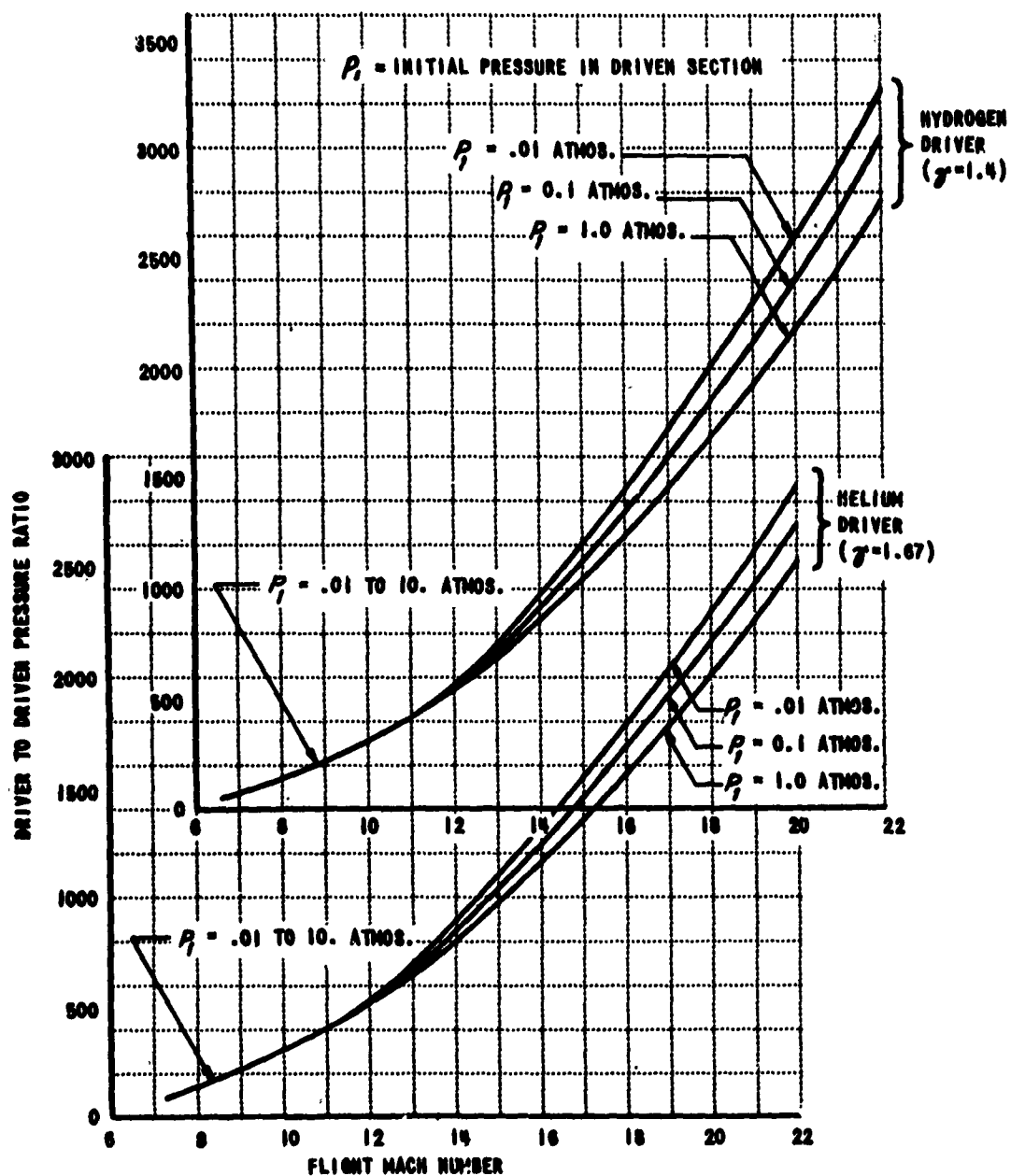


Figure 25a - Required diaphragm pressure ratio for tailoring at various flight Mach numbers (unsteady configuration). (Ref. 39)

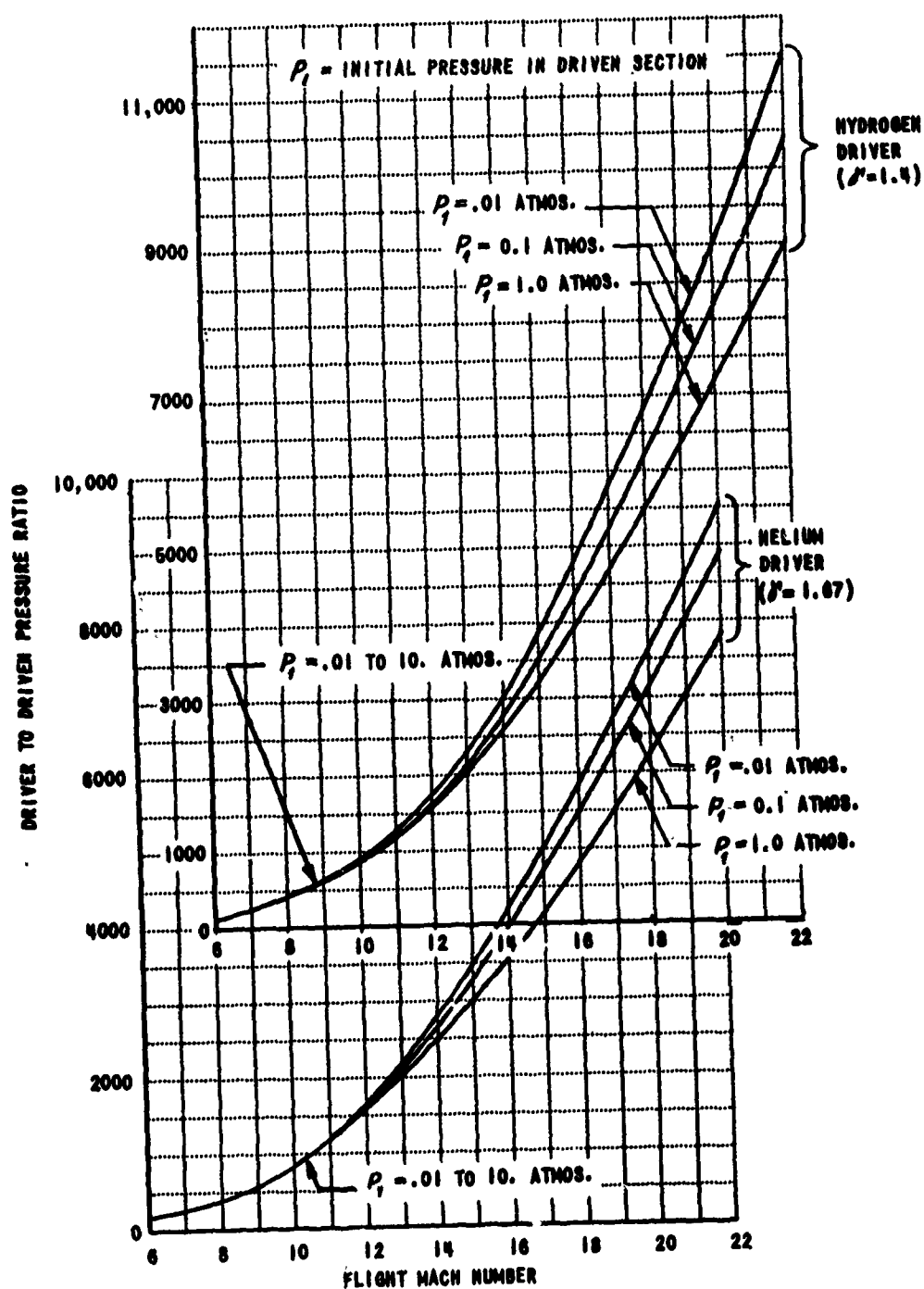


Figure 25b - Required diaphragm pressure ratio for tailoring at various flight Mach numbers (steady configuration). (Ref. 39)

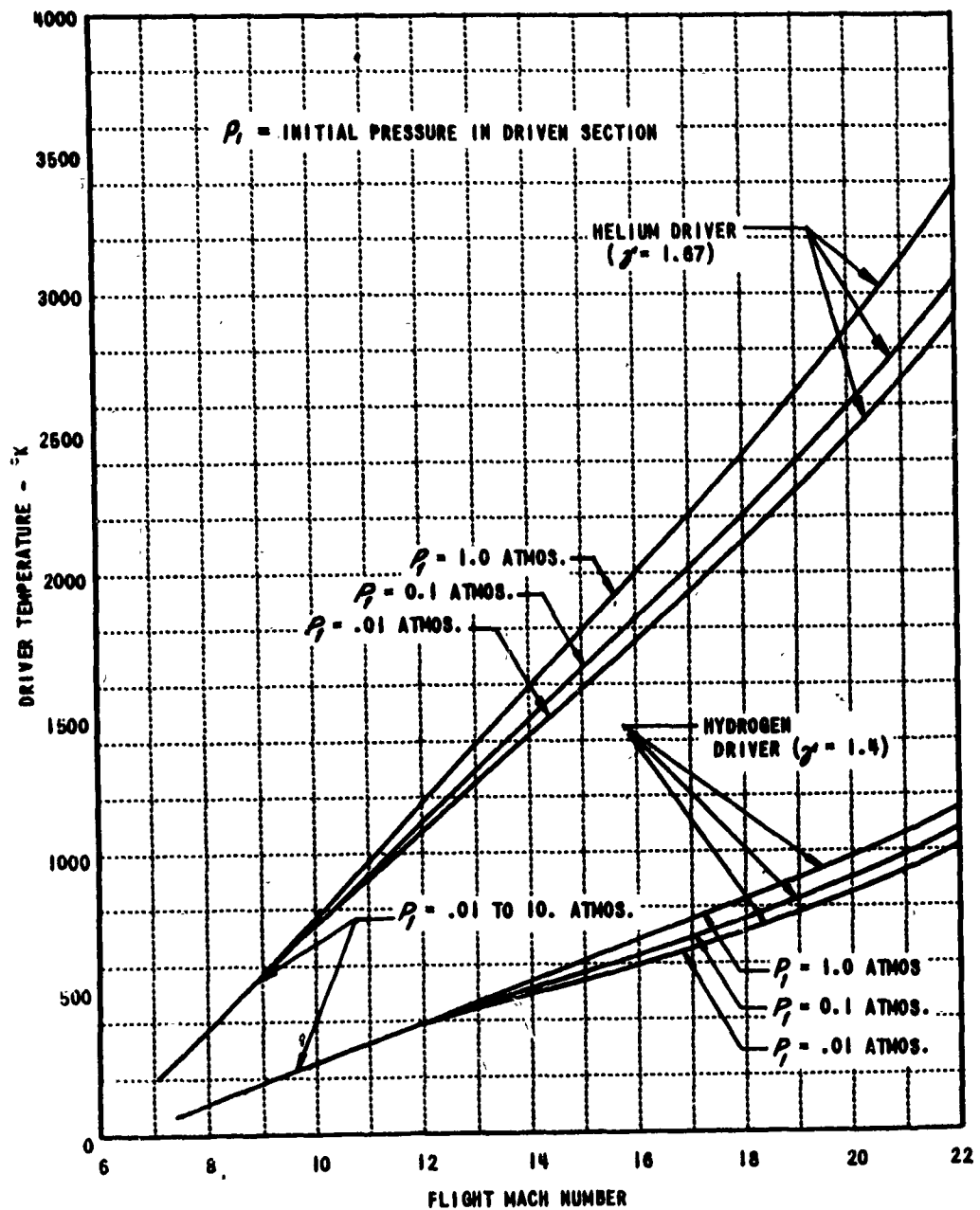


Figure 26a - Required initial driver gas temperature for tailoring at various flight Mach numbers (steady configuration). (Ref. 39)

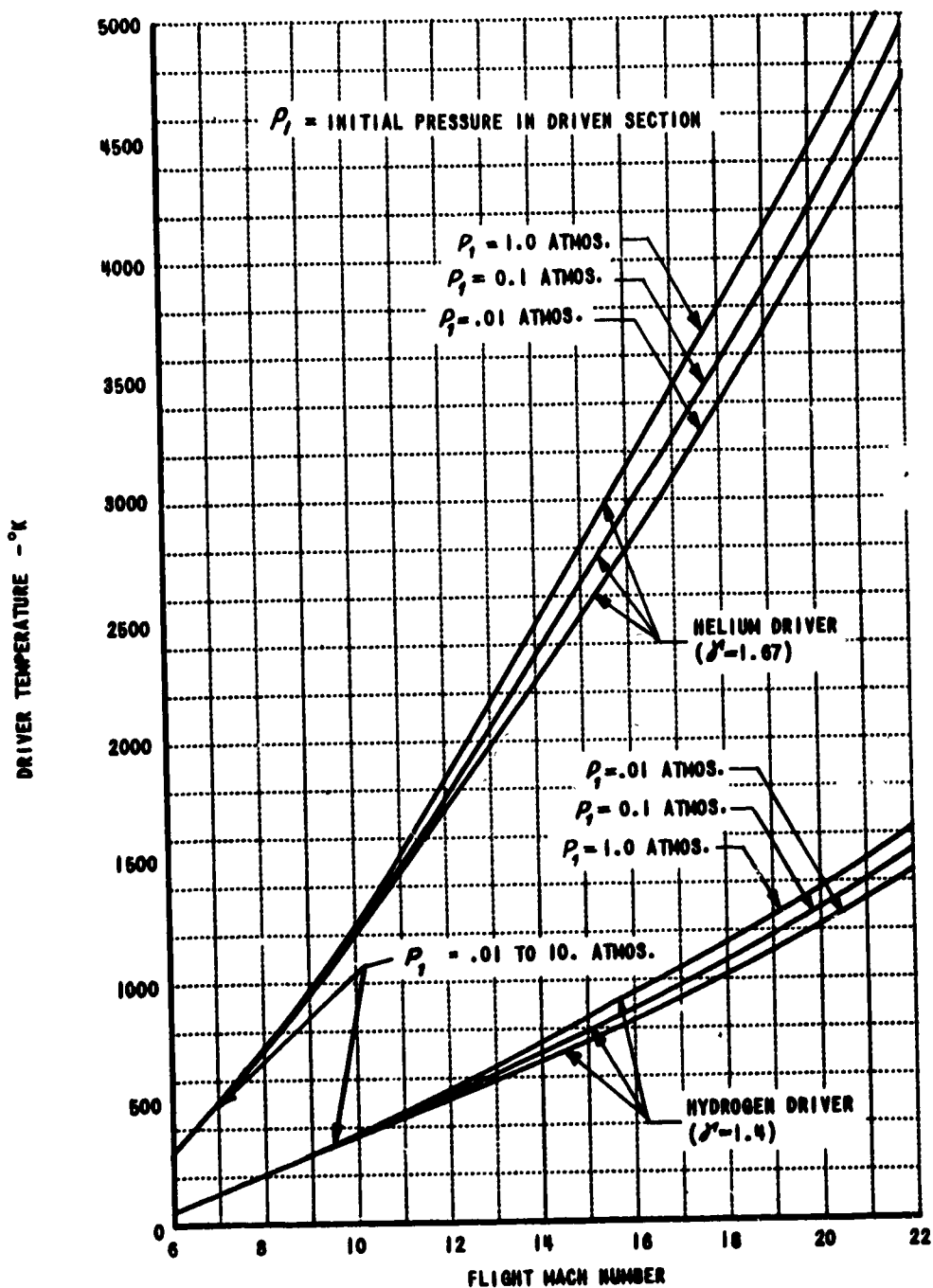


Figure 26b - Required initial driver gas temperature for tailoring at various flight Mach numbers (steady configuration). (Ref. 39)

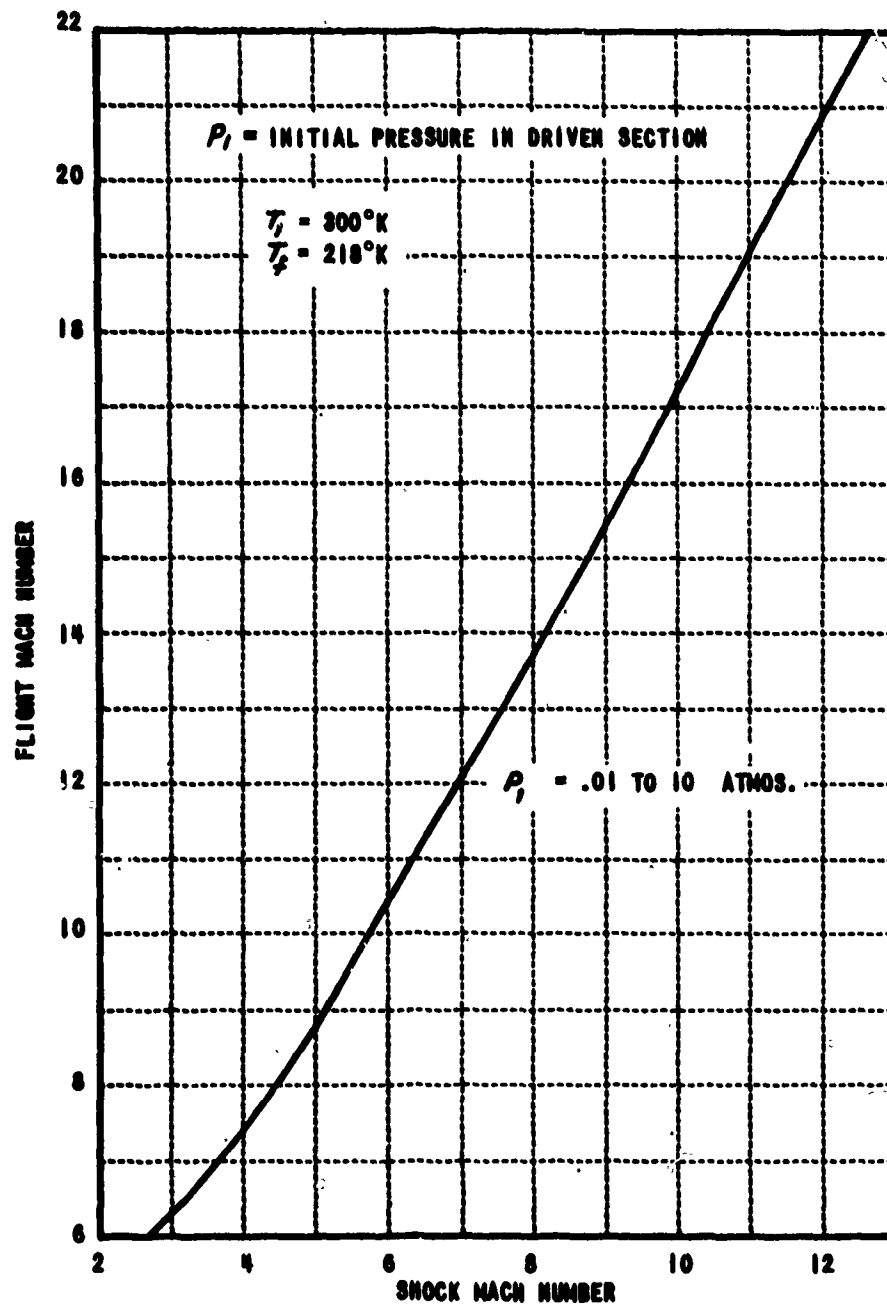


Figure 27 - Variation of flight Mach number with shock Mach numbers. (steady configuration). (Ref. 39)

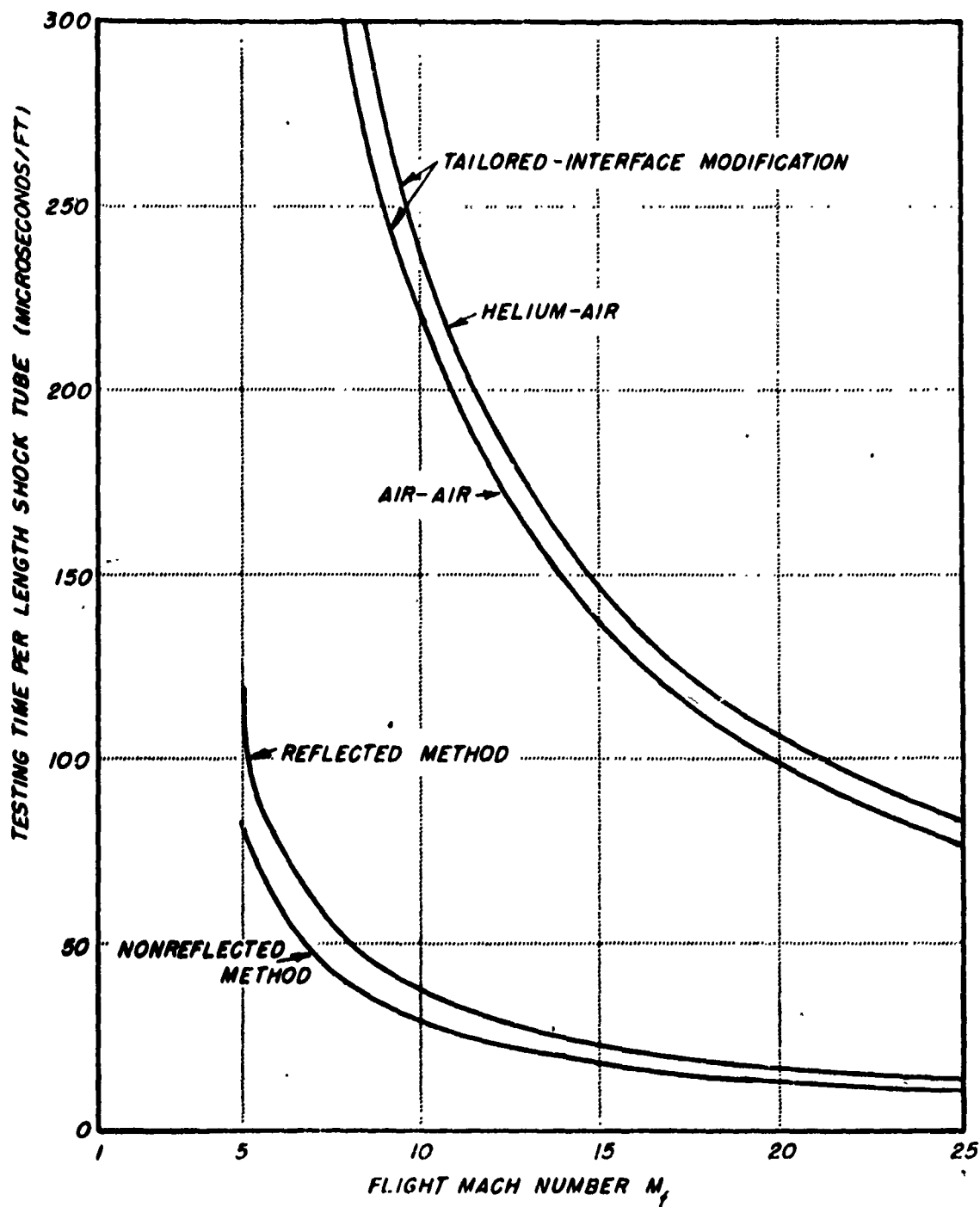


Figure 28a - Testing time for four modifications. (Ref. 37)

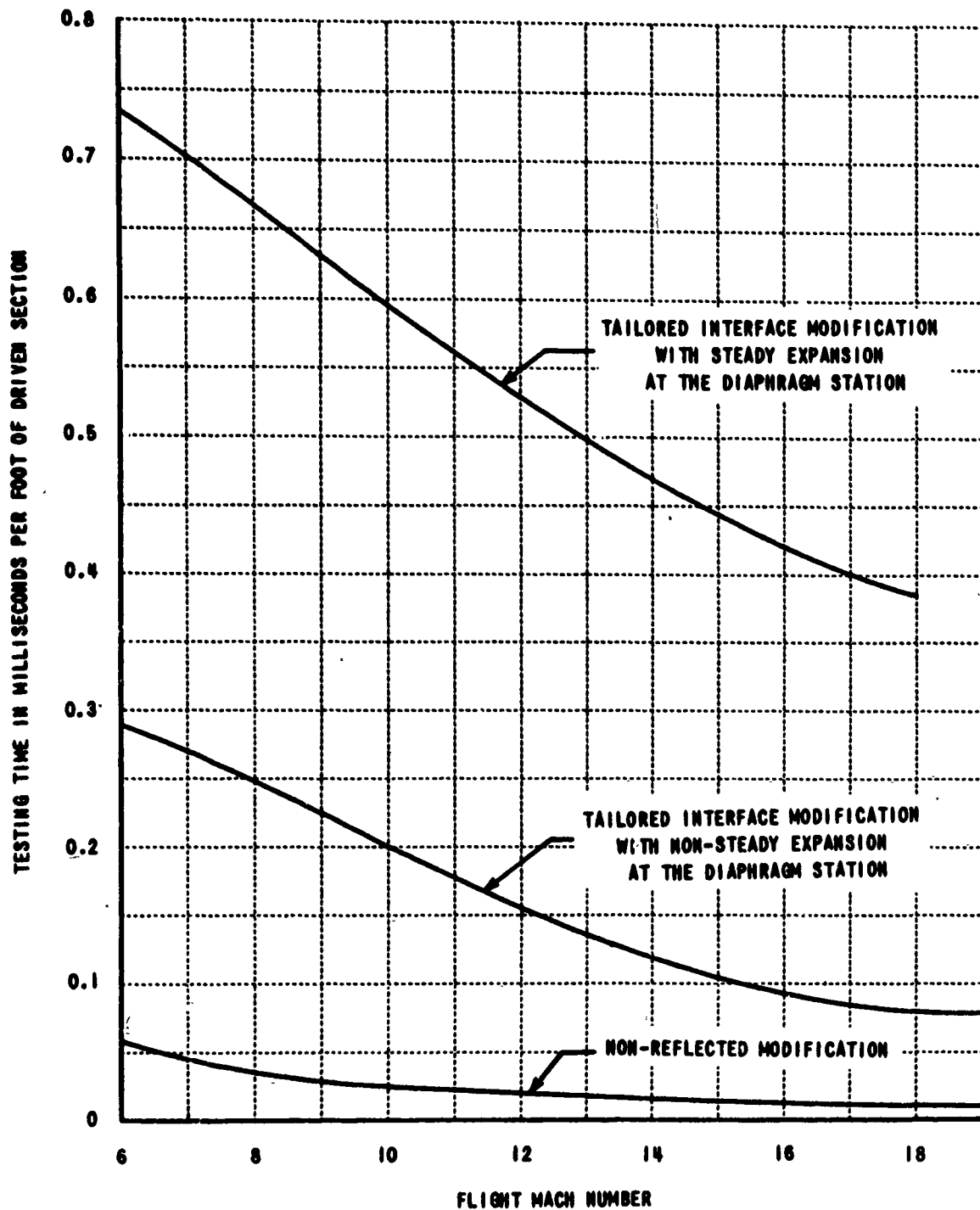


Figure 28b - Nominal testing time of hypersonic shock tunnel modifications based on equilibrium real gas calculations. (Ref. 12)

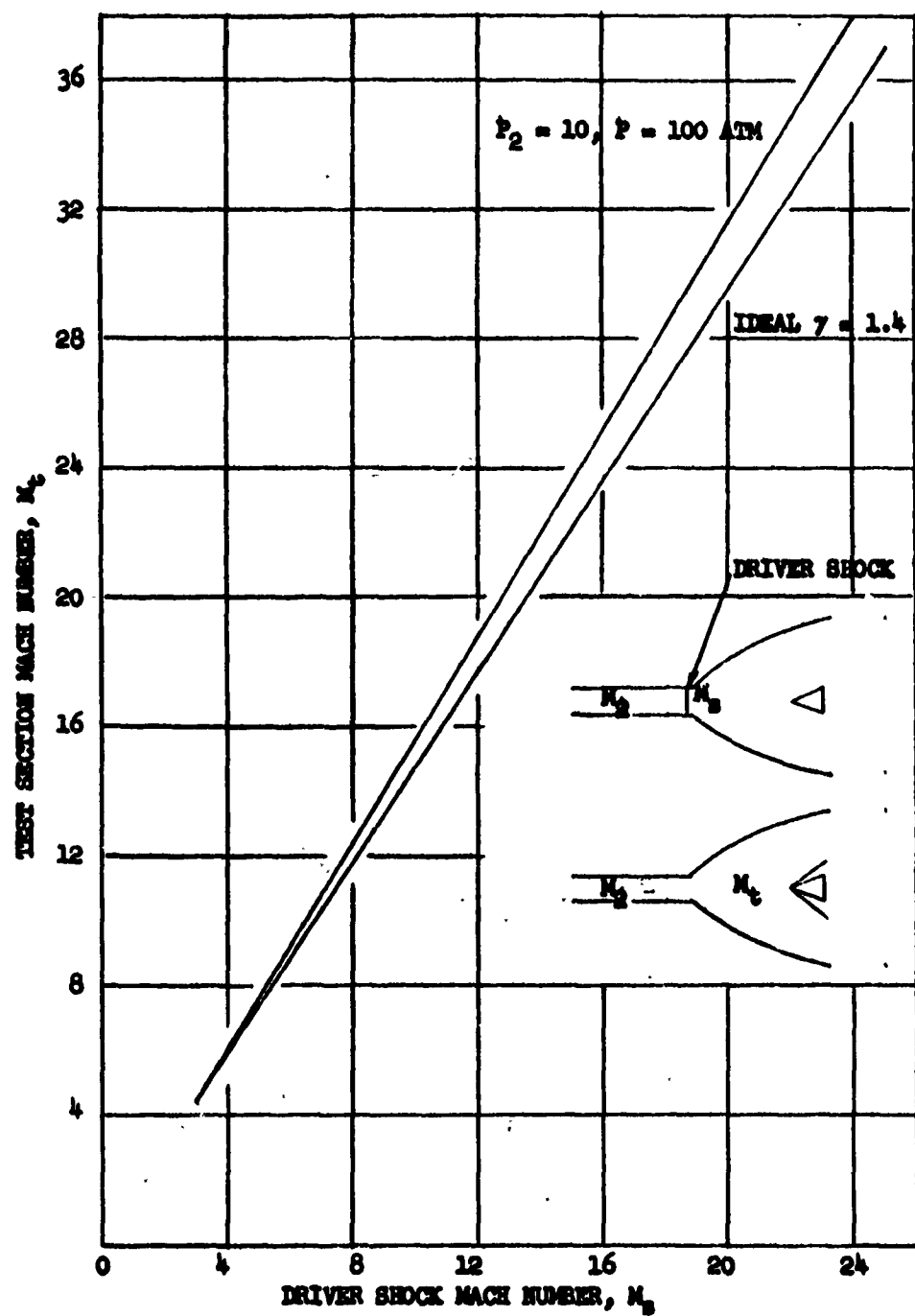


Figure 29 - Variation of Test Section Mach number with driver shock Mach number. (Ref. 14)

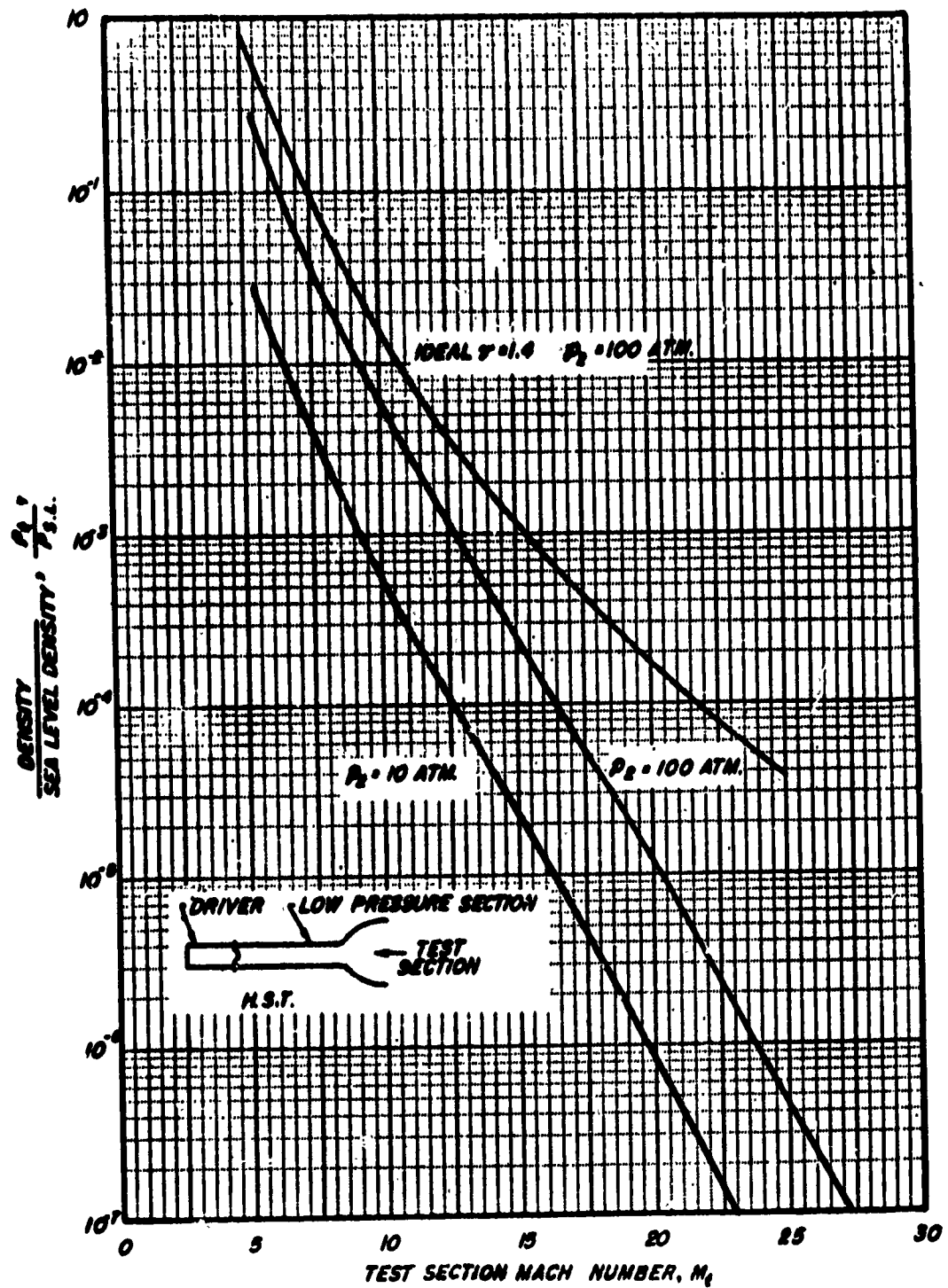


Figure 30 - Density in test section of hypersonic shock tunnel vs. test section Mach number. (Ref. 14)

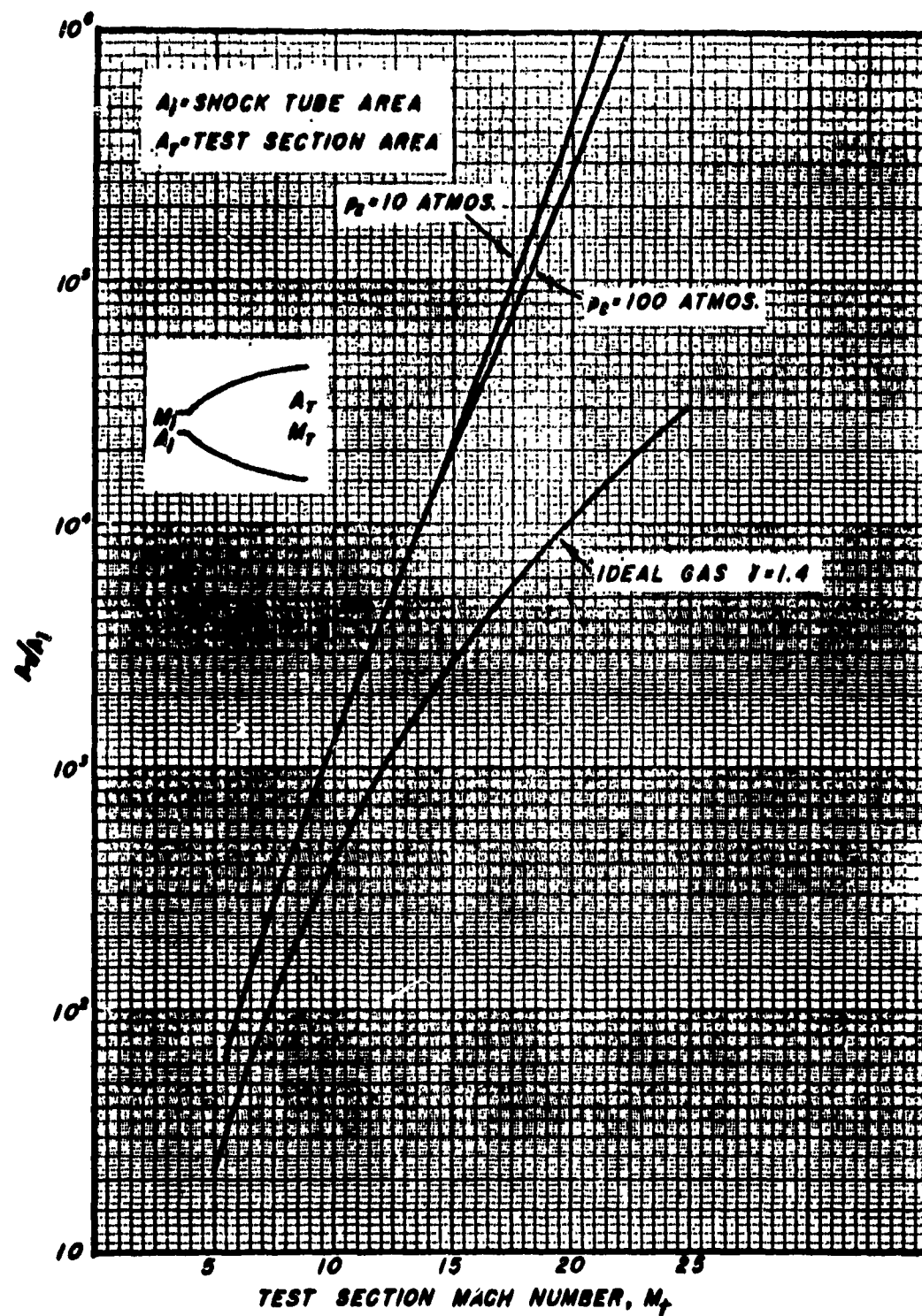


Figure 31 - Expansion of the hypersonic shock tunnel vs. test section Mach number (Ref 14)

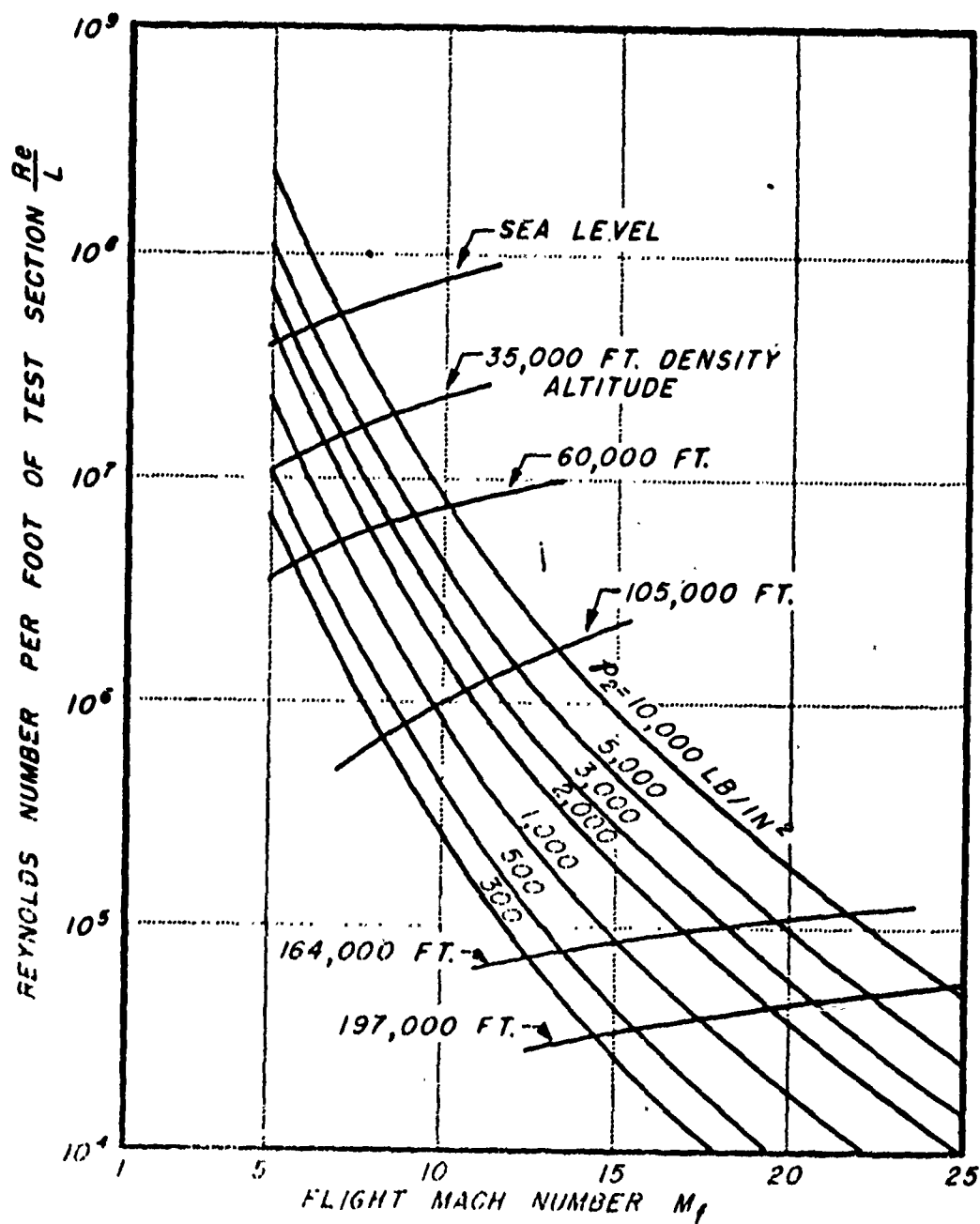


Figure 32 - Performance of the nonreflected method, $\gamma = 1.4$, $T_1 = 518.4^\circ\text{R}$, $T_2 = 391.6^\circ\text{R}$, $R = 1716 \text{ FT}^2/\text{SEC}^2$, p_2 = static pressure behind the incident shock (LB/IN^2) (Ref. 37)

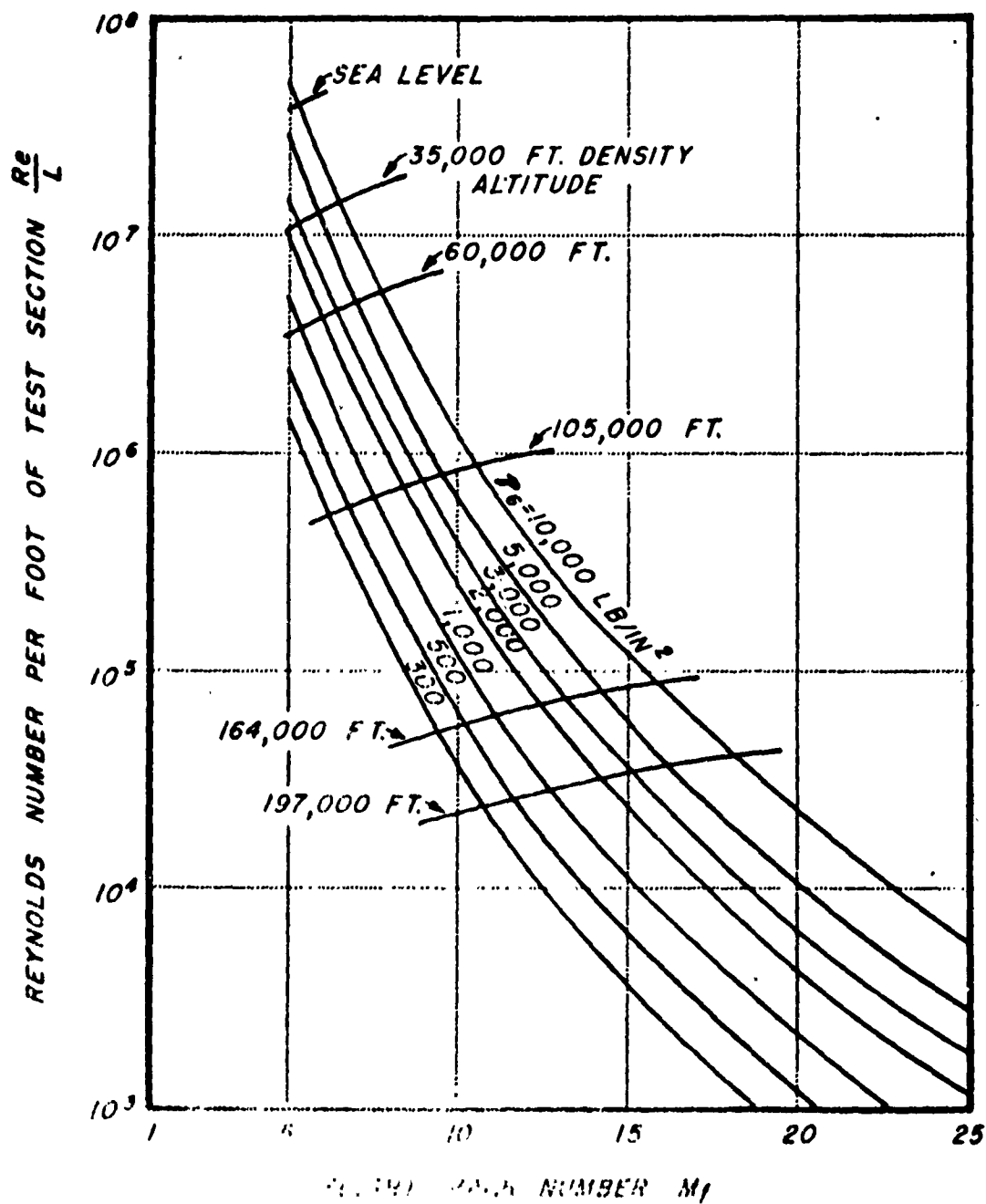


Figure 33 - Performance of the reflected method $T_1 = 518.4^\circ R$,
 $T_f = 391.8^\circ R$, $R = 1716 \text{ FT}^2/\text{SEC}^2$ OR, p_6 = static pressure
 behind the reflected shock (LB/IN²) (Ref. 37)

He/Air, $P_{14} = 0$, $\alpha = 6$, $\beta = 1/7$

	P_{21}	Γ_{34}	A_{3-}	T_{3+}	Γ_{21}	A_{21}	T_{21}	M_3	U_{34}	U_{21}	M_2	M_3	C_{34}
0	∞	x	x	x	6	∞	∞	∞	x	∞	1.89	x	x
0.1	0.22	0	0	0	5.92	8.45	71.4	19.0	5	15.8	1.87	∞	5
1.0	0.4	0	0	0	5.30	2.88	8.30	6.16	5	5.0	1.73	∞	5

x indeterminate

He/Air, $P_{14} = 0$, $\alpha_1 = 6$, $\beta_1 = 1/7$, $\alpha_4 = 4$, $\beta_4 = 1/5$, $T_4 = T_1$

	P_{21}	Γ_{34}	A_{3-}	T_{3+}	Γ_{21}	A_{21}	T_{21}	M_3	U_{34}	U_{21}	M_2	M_3	C_{34}
.231	132	0	0	0	5.75	4.79	23.0	10.6	3.00	8.83	1.64	∞	3

He/Air, $P_{14} = 0$, $\alpha = 6$, $\beta = 1/7$, $T_4 = T_1$

	P_{21}	Γ_{34}	A_{3-}	T_{3+}	Γ_{21}	A_{21}	T_{21}	M_3	U_{34}	U_{21}	M_2	M_3	C_{34}
.0755	575	0	0	0	5.94	9.82	96.5	22.2	5	18.5	1.88	∞	5

Table 1 - Flow quantities for very strong shock waves.

P_0	10	10^2	10^3	10^4	10^5
M_s max.	1.64	2.68	4.39	7.20	11.79

TABLE 2

MAXIMUM SHOCK MACH NUMBERS FOR MULTIPLE DIAPHRAGM SHOCK TUBES (Ref. 9)

	Driver - Driven Gas Combinations	A_4/A_1			
		1	1.51	2.25	∞
$T_{41} = 1$	N_2/N_2	6.18	6.34	6.47	6.76
	N_2/A	7.48	7.69	7.84	8.20
	He/N_2	10.9	11.3	11.6	12.5
	He/A	12.8	13.3	13.7	14.7
	H_2/N_2	22.6	23.2	23.6	24.7
	H_2/A	27.5	28.3	28.8	30.1
$T_{41} = 2$	He/N_2	14.8	15.4	15.9	17.1
	He/A	18.0	18.8	19.3	20.8
	H_2/N_2	31.9	32.8	33.4	34.9
	H_2/A	38.9	40.0	40.7	42.6

TABLE 3

MAXIMUM VALUES OF SHOCK MACH NUMBER, M_s FOR $P_{41} \rightarrow \infty$ (Ref. 10)